Astronomy & Astrophysics manuscript no. rejkuba February 3, 2008
(DOI: will be inserted by hand later)

Dwarf elliptical galaxies in Centaurus A group: stellar populations in AM 1339-445 and AM 1343-452⋆ ⋆⋆

M. Rejkuba[1], G. S. Da Costa[2], H. Jerjen[2], M. Zoccali[3], and B. Binggeli[4]

[1] European Southern Observatory, Karl-Schwarzschild-Strasse 2, D-85748 Garching, Germany
E-mail: mrejkuba@eso.org
[2] Research School of Astronomy and Astrophysics, Institute of Advanced Studies, Australian National University, Cotter Road, Weston Creek, ACT 2611, Australia
E-mail: [gdc, jerjen]@mso.anu.edu.au
[3] Department of Astronomy and Astrophysics, Pontificia Universidad Católica de Chile, Vicuña Mackenna 4860, Santiago 22, Chile
E-mail: mzoccali@astro.puc.cl
[4] Astronomy Department, University of Basel, Venusstrasse 7, Basel, Switzerland
E-mail: binggeli@astro.unibas.ch

23 September 2005 / 23 November 2005

Abstract. We study the red giant populations of two dE galaxies, AM 1339-445 and AM 1343-452, with the aim of investigating the number and luminosity of any upper asymptotic giant branch (AGB) stars present. The galaxies are members of the Centaurus A group (D ≈ 3.8 Mpc) and are classified as outlying (R ≈ 350 kpc) satellites of Cen A. The analysis is based on near-IR photometry for individual red giant stars, derived from images obtained with ISAAC on the VLT. The photometry, along with optical data derived from WFPC2 images retrieved from the HST science archive, enable us to investigate the stellar populations of the dEs in the vicinity of the red giant branch (RGB) tip. In both systems we find stars above the RGB tip, which we interpret as intermediate-age upper-AGB stars. The presence of such stars is indicative of extended star formation in these dEs similar to that seen in many, but not all, dEs in the Local Group. For AM 1339-445, the brightest of the upper-AGB stars have M_{bol} ≈ –4.5 while those in AM 1343-452 have M_{bol} ≈ –4.8 mag. These luminosities suggest ages of approximately 6.5 ± 1 and 4 ± 1 Gyr as estimates for the epoch of the last episode of significant star formation in these systems. In both cases the number of upper-AGB stars suggests that ∼15% of the total stellar population is in the form of intermediate-age stars, considerably less than is the case for outlying dE satellites of the Milky Way such as Fornax and Leo I.

Key words. Galaxies: dwarf – Galaxies: stellar content – Galaxies: evolution – Stars: AGB and post-AGB

1. Introduction

Dwarf elliptical and dwarf spheroidal galaxies (we will refer to both classes as dwarf elliptical (dE) galaxies from now on) are often assumed to have simple star formation histories because, at the present epoch, they generally lack neutral hydrogen and show no current or very recent star formation. These properties separate them, morphologically, from the gas-rich, star-forming dwarf irregular (dIrr) galaxies. However, detailed studies of resolved stellar populations in Local Group (LG) dEs have revealed a surprising diversity of star formation histories, with some LG dEs containing stars as young as ∼1 Gyr, or perhaps even younger (e.g. Fornax and Leo I; see reviews by Da Costa 1997; Mateo 1998; van den Bergh 1999, 2000; Grebel 2000).

The dwarf galaxies in the LG follow a morphology-density relation in that the dEs are preferentially close to the Milky Way (MW) or M31, the two most massive galaxies in the LG, while almost all of the dIrr galaxies are located in the outskirts of the LG in more isolated regions. Further, among the MW and M31 dE satellite galaxies, there is a tendency for the systems that lie at larger distances to have larger intermediate-age (i.e. age ≈ 1–10 Gyr) populations (e.g. van den Bergh 1994). This has led to the conjecture that proximity to a luminous galaxy, and the type of that galaxy, can play an important role in defining dwarf galaxy evolution. In particular, externally driven processes such as ram-pressure stripping by the hot gaseous halo

Send offprint requests to: M. Rejkuba

⋆ Based on observations collected at the European Southern Observatory, Paranal, Chile, within the Observing Programme 073.B-0131, and on observations made with the NASA/ESA *Hubble Space Telescope*, obtained from the data archive at the Space Telescope Science Institute. STScI is operated by the Association of Universities for Research in Astronomy, Inc., under NASA Contract NAS 5-26555.

⋆⋆ Tables 2 and 3 are only available in electronic form at the CDS via anonymous ftp to cdsarc.u-strasbg.fr (130.79.128.5) or via http://cdsweb.u-strasbg.fr/cgi-bin/qcat?J/A+A/../..

of a massive galaxy, and/or tidal effects, may control the rate at which gas is lost from a dwarf system, and thus its star formation history. This approach has support from numerical simulations (e.g. Mayer et al. 2001). Grebel et al. (2003) also argue that external gas removal mechanisms are required to generate low-luminosity dEs, though they suggest that the transition-type dwarfs, i.e. the dwarfs classified as dIrr/dE, are the best model for low luminosity dEs that have not lost their gas, rather than dIrrs.

However, the model in which the evolution of a dwarf system is halted by externally induced gas loss, does not easily explain the existence of LG dEs like Tucana and Cetus. These dwarfs show very little, if any, evidence for extended star formation despite having isolated locations far from the MW or M31 (e.g. Da Costa 1998; Sarajedini et al. 2002). If these dEs have always remained isolated, then an internal process must have been responsible for the apparent complete gas loss at early times.

In order to explore further the importance of external vs. internal processes in driving the star formation in these small systems, it is necessary to study in detail dE galaxies in environments different from that of the LG. The relatively nearby Centaurus A Group (D ≈ 3.8 Mpc) is one such environment. This group, which has the unusual giant E galaxy Cen A as its single dominant member, is more compact than the LG and it probably contains perhaps twice as many galaxies. For instance, Karachentsev et al. (2002) list 13 galaxies that are most likely within a 600 kpc radius of Cen A, and which are brighter than $M_B \approx -12$. Besides Cen A itself, these include the giant galaxies NGC 4945 and NGC 5102 as well as 10 dwarf galaxies, 6 of which are early-type and 4 late-type. This catalogue is likely to be significantly incomplete. In contrast, in the Local Group, for an approximately equivalent volume centered on the LG barycentre and with an equivalent magnitude cutoff, the compilation of van den Bergh (2000) yields a (complete) sample of 13 galaxies: 4 large galaxies (MW, M31, M33 and the LMC), 6 early-type dwarfs (M32, NGC 205, NGC 185, NGC 147, Fornax and Sagittarius) and 3 late-type dwarfs (SMC, IC10 and IC1613). Thus it is likely that the Cen A group has provided a significantly different environment for its dwarf members than has the LG.

We have begun a program to study the red giant populations of the dE galaxies in the Cen A group, with the ultimate aim of investigating the extent to which star formation history indicators correlate with distance from the dominant galaxy of the group, Cen A. Specifically, we will investigate the number and luminosity of upper-AGB stars in the dE galaxies. Upper-AGB stars are stars with sufficient mass to evolve to luminosities above the RGB tip, and their presence, provided the system is relatively metal-poor ($\langle$[Fe/H]$\rangle \leq -1.0$), as is the case for all but the most luminous dEs, is an unambiguous indicator of the existence of an intermediate-age (~1–10 Gyr) population. The luminosity of the brightest upper-AGB stars is also a measure of the age of the youngest intermediate population of significance. Because of their cool effective temperatures, these upper-AGB stars are best studied in the near-infrared. Indeed it was near-IR observations that provided the first evidence for the diversity of star formation histories among the MW dSph companions (cf. Aaronson & Mould 1980).

Table 1. Fundamental parameters of the two target dE galaxies in Cen A group.

Name	AM 1339-445	AM 1343-452	
$\alpha_{J2000.0}$	13:42:05.8	13:46:18.8	
$\delta_{J2000.0}$	−45:12:21	−45:41:05	
Type	dE	dE	1
B_T (mag)	16.32	17.57	1
R_T (mag)	14.76	16.02	1
$(B-R)_0^T$ (mag)	1.38	1.35	1
$r_{\rm eff,R}$ (arcsec)	23.8	14.7	1
$\langle\mu\rangle_{\rm eff,R}$	23.63	23.85	1
E$(B-V)$ (mag)	0.111	0.121	2
$(m-M)_0$ (mag)	27.87 ± 0.27	27.99 ± 0.37	1 (SBF)
	27.77 ± 0.21	27.92 ± 0.25	3 (TRGB)
	27.74 ± 0.20	27.86 ± 0.20	4 (TRGB)
$\langle$[Fe/H]$\rangle$	−1.4 ± 0.2	−1.6 ± 0.2	4
References:	1: Jerjen et al. (2000b); 2: Schlegel et al. (1998); 3: Karachentsev et al. (2002); 4: this work		

Using the ISAAC near-IR array at the ESO Very Large Telescope (VLT) we have obtained J_s and K_s-band images of 14 Cen A group dwarf galaxies. The full data set, together with description of the reduction and analysis techniques, will be presented in a forthcoming paper (Rejkuba et al., in preparation). We present here the first results of our program – analysis of the resolved red giant stellar populations of two Cen A group dE galaxies, AM 1339-445 (KK 211) and AM 1343-452 (KK 217). For these two galaxies it is possible to supplement the near-IR data with V and I band WFPC2 images from the HST science archive, permitting estimates of the distances and of the average metallicity of their stars.

In Table 1 we summarize the fundamental parameters of the two dwarf ellipticals. The last column gives the literature reference for the tabulated data.

Using the integrated magnitudes of Jerjen et al. (2000a) and the reddenings and moduli adopted here (see Table 1 and following sections) the absolute blue magnitudes of these two galaxies are $M_B = -11.9$ and -10.8, respectively, with colours $(B-R)_0 = 1.38$ and 1.35, typical for dE galaxies (e.g. Evans et al. 1990). Neither galaxy is detected in the HIPASS survey: the 3-σ upper limits on their HI contents correspond to $2.8 \times 10^6 M_\odot$ and $3.1 \times 10^6 M_\odot$, respectively, for an assumed 10 kms^{-1} line width and detection limits of the survey from Barnes et al. (2001). Karachentsev et al. (2002) list line-of-sight distances for the two galaxies based on the I magnitude of the red giant branch tip (see also Sect. 3.3). With those distances, the angular separations from Cen A, and a distance for Cen A of 3.84 Mpc (Rejkuba 2004), the true separation of AM 1339-445 from Cen A is ~390 kpc, while that of AM 1343-452 is approximately 320 kpc. Karachentsev et al. (2002) label both dwarfs as companions of Cen A. The distances of both these dEs from Cen A are therefore somewhat larger than those of the outer dE satellites Leo I and Leo II from the MW, and those of the outer dE satellites And II, And VI (Peg) and And VII (Cas) from M31.

The paper is organised as follows. In the following section the observations and reductions are described, first for the near-IR data and then for the WFPC2 data. The third section outlines the analysis of the resulting colour-magnitude diagrams (CMDs) for the two dwarfs. The fourth section discusses the results, which are summarised in the final section. A preliminary description of this work has appeared in Da Costa (2005) and Rejkuba et al. (2005).

2. Observations and reductions

The observations and the subsequent photometry of the ISAAC frames are summarized in Sect. 2.1. More details of the reduction and analysis techniques will be presented in a forthcoming paper (Rejkuba et al., in preparation), together with the photometry of the remaining 12 Cen A group dwarf galaxies in our sample.

The optical images of our program galaxies come from the HST WFPC2 'snapshot' programme 8192 (PI: Seitzer), and have been discussed in Karachentsev et al. (2002). These authors were primarily interested in distances, derived from the tip of the RGB, to establish, or confirm, membership in the Cen A group for a sizeable sample of dwarfs of all types. For both dEs discussed here, however, Jerjen et al. (2000b) had previously established Cen A group membership via a distance determined with the surface brightness fluctuation method. Since Karachentsev et al. (2002) did not publish their photometry for individual stars, we retrieved the WFPC2 data frames from the HST science archive and carried out our own photometric analysis. This is described in Sect. 2.2. We then repeat the distance analysis and use the CMDs to infer the average metallicity of the dE stars and to search for candidate upper-AGB stars.

The combination of the WFPC2 and ISAAC photometry is described in Sect. 2.3 and the final catalogue is available as an electronic table from CDS. We note that in order to correct our photometry for Galactic extinction, we use the following E(B − V) values throughout the paper (cf. Table 1): $E(B-V)_{AM1339-445} = 0.111$ and $E(B-V)_{AM1343-452} = 0.121$ (Schlegel et al. 1998). We adopt $A_V = 3.3E(B-V)$ and the $E(V-I)$, $E(B-V)$ relation from Dean et al. (1978), while the Cardelli et al. (1989) extinction law is used to calculate A_J and A_K values.

2.1. ISAAC data

The Near-IR observations of AM 1339-445 and AM 1343-452 were taken in service mode using the short wavelength arm of the ISAAC instrument on the Antu (UT1) Very Large Telescope (VLT) at ESO Paranal Observatory. The field-of-view is $2\farcm5 \times 2\farcm5$ and the pixel scale $0\farcs148$.

Each galaxy was observed once in the J_s and twice in the K_s-band. AM 1339-445 was observed on July 19, 2004 in the J_s band, and the two K_s-band epochs were secured on May 10 and May 14, 2004. The J_s and one K_s epoch of AM 1343-452 were taken on June 27, 2004, and the other K_s observation on May 14, 2004. Each observation consisted of a sequence of jittered short exposures. The total exposure times were 2352 sec for each K_s observation and 2100 sec for J_s.

The standard procedure in reducing infrared (IR) data consists of dark subtraction, flat-field correction, sky subtraction, registering and combining the images. The details of the adopted data reduction procedures within IRAF are described in Rejkuba et al. (2001). At the end of the reduction all the images taken within each individual jittered sequence were combined. From now on, when we refer to an image in the J_s, or K_s-band, we always mean these combined sequences. All the images have very high resolution thanks to excellent seeing. For example, on the K_s band images of both galaxies taken on May 14, 2004, we measure FWHM of only $0\farcs33$, while the J_s-band images have slightly worse resolution, with seeing of $0\farcs58$.

Point-spread-function (PSF) fitting photometry on the reduced images was done using the suite of DAOPHOT, ALLSTAR and ALLFRAME programmes (Stetson 1987, 1994). We combined the J_s and K_s images of each galaxy to derive the master star list, which was then used to obtain photometry from the J_s and the two K_s images. The final photometric catalogue for each galaxy contains all the sources that could be measured in both J_s and at least one K_s-band image and that had photometric errors, measured by ALLFRAME, smaller than 0.3 mag, and PSF fitting quality parameters $\chi \leq 1.5$ and |sharpness| < 2. After this selection the catalogues contain 826 stars in the field centered on AM 1339-445 and 743 stars in AM 1343-452.

Photometric calibration was done by applying the zero point difference between our instrumental magnitude measurements and magnitudes of stars found in common with the 2MASS all-sky catalog of point sources (Cutri et al. 2003), as previous experience with this instrumental system has shown that any colour terms are negligible. The respective J_0 vs. $(J-K)_0$ and K_0 vs. $(J-K)_0$ CMDs are shown in Fig. 1 and 2. The brighter parts of the CMDs are dominated by field stars, many of which have similar $(J-K)_0$ colours. Stars found in common with the 2MASS catalog, and used for calibration, are among the brightest of these field stars. The contribution to the CMDs from the galaxy stars are found at the fainter magnitudes.

Completeness and magnitude errors were measured using artificial-star tests, which are discussed in more detail in the paper that describes the whole dataset (Rejkuba et al., in preparation). Specifically, the tests show that for these galaxies, the completeness and the magnitude errors as a function of magnitude vary very little across the field, indicating that there are no problems with crowding in the centers of the images. The 50% completeness limit is reached at $J_0 = 22.8$ and $K_0 = 21.8$ in AM 1339-445, and $J_0 = 23.0$ and $K_0 = 22.0$ in AM 1343-452. These completeness limits are indicated on CMDs in Fig. 1 and 2 with dashed lines. Typical error-bars, computed as average difference between input and recovered magnitudes as a function of input magnitude in completeness simulations, are also plotted. The errors for colour typical of RGB stars and magnitudes close to the RGB tip as well as one magnitude brighter are quoted in the captions of these figures.

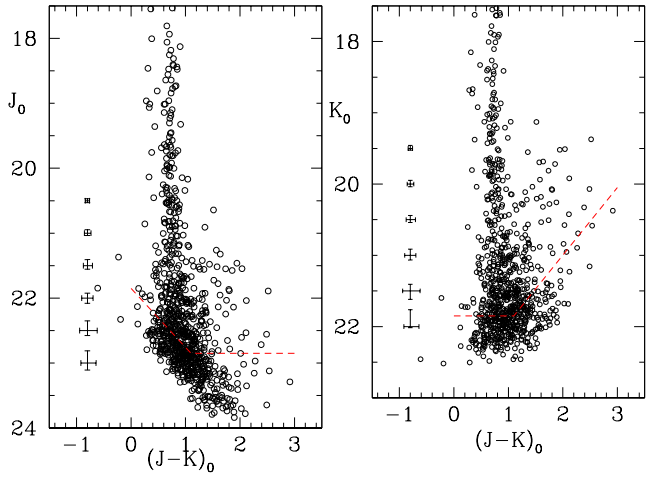

Fig. 1. AM 1339-445 near-IR CMDs. Dashed lines indicate 50% completeness limits, and the typical error-bars are indicated on the left side. For example, at $K_0 = 21.5$ and $(J-K)_0 = 1.0$ they amount to $\sigma_K = 0.2$ and $\sigma_{(J-K)} = 0.3$, while one magnitude brighter, at $K_0 = 20.5$, and at the same colour, they are $\sigma_K = 0.09$ and $\sigma_{(J-K)} = 0.15$.

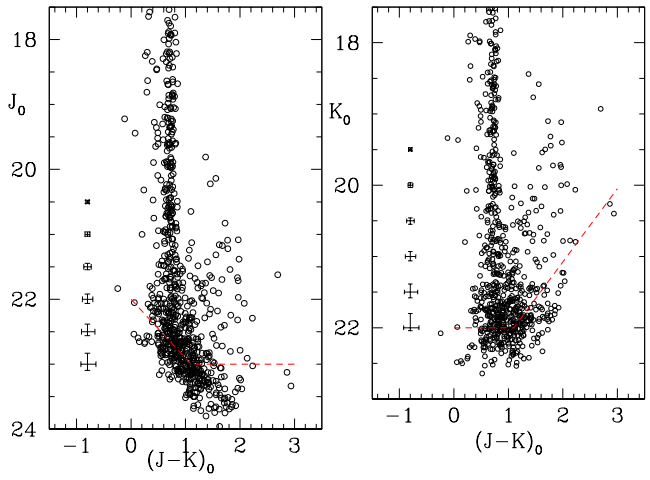

Fig. 2. AM 1343-452 near-IR CMDs. Dashed lines indicate 50% completeness limits, and the typical error-bars are indicated on the left side. For example, at $K_0 = 21.5$ and $(J-K)_0 = 1.0$ they amount to $\sigma_K = 0.15$ and $\sigma_{(J-K)} = 0.25$, while one magnitude brighter, at $K_0 = 20.5$, and at the same colour, they are $\sigma_K = 0.08$ and $\sigma_{(J-K)} = 0.12$.

2.2. HST data

The HST WFPC2 data for each galaxy consists of single 600 sec exposures through the $F606W$ ('Wide-V') and $F814W$ ('Wide-I') filters. The pipeline-processed image files and the accompanying data quality files were retrieved from the HST science archive. In both cases the galaxy was centered on the WF3 chip. The images were analysed with the December 2004 version (version 1.1.7a) of Dolphin's HSTphot package (Dolphin 2000b). For each galaxy, the data quality files were first used to mask bad pixels and other defects in the images.

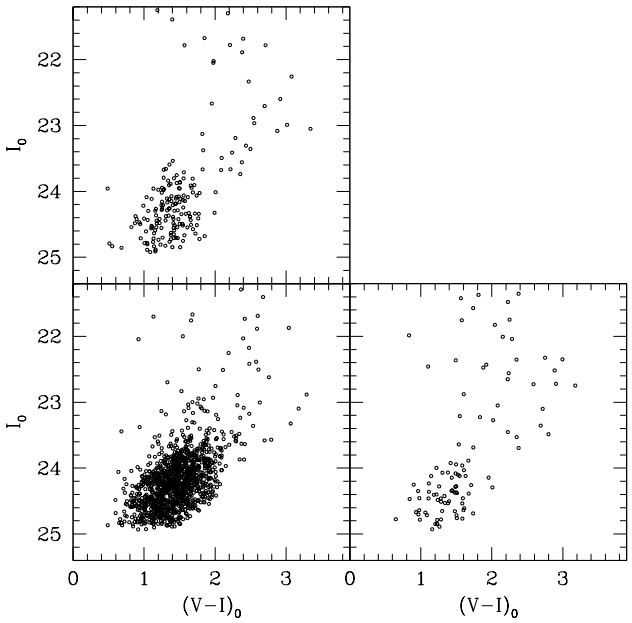

Fig. 3. Reddening corrected CMDs for AM 1339-445 from the WFPC2 data. WF2 is the upper-left, WF3 is the lower-left and WF4 is the lower-right.

The 'sky' image was then computed with the *getsky* routine and the *crmask* code used in conjunction with both images to remove cosmic rays. Finally, the *HSTphot* code was run to produce V and I photometry for all objects detected on both images. This code includes updated CTE corrections and zero-point calibrations (cf. Dolphin 2000b). Because of the small number of stars on the PC1 frames, the data from that chip were omitted from the further analysis.

The output of *HSTphot* contains a number of parameters for each detected object. These include a classification, χ, sharpness and roundness parameters, errors in the final magnitude, and estimates of the effect of crowding. In order to produce as clean a CMD as possible, only objects with a classification of 1 ('good star') were retained. Further, stars with discrepant χ, sharpness, roundness and errors for their magnitude were discarded. Similarly, any star with a crowding parameter exceeding 0.05 mag was excluded. The reddening corrected CMDs for the two galaxies are shown in Fig. 3 for AM 1339-445, and Fig. 4 for AM 1343-452. It is immediately apparent that the galaxy stars are primarily confined to the WF3 chip, though there are indications that galaxy stars also populate the other chips to some extent, particularly WF2 for AM 1339-445.

2.3. Combined data

While the total WFPC2 field is comparable to that of the ISAAC data, it is evident from Figs. 3 and 4 that the bulk of the red giants are contained on the WF3 chip. The centres of the two galaxies are in the centre of the ISAAC and of the WF3 chip, while the overlap between WF2 and WF4 chips and the ISAAC field of view is much smaller, as can be seen from

Table 2. Combined WFPC2 and ISAAC measurements in V, I, J_s and the average K_s magnitude of all the stars in AM 1339-445 without extinction correction. For each magnitude in parenthesis we give magnitude errors as given by photometric package, HSTphot and DAOPHOT. Here we give only the first three entries, and the complete table is available through the CDS.

ID	X(WF3)	Y(WF3)	$V(\pm\sigma)$	$I(\pm\sigma)$	$J_s(\pm\sigma)$	$K_s(\pm\sigma)$
226	151.61	731.13	21.486 (0.010)	19.551 (0.007)	18.29 (0.01)	17.49 (0.01)
234	129.33	701.22	26.027 (0.126)	24.248 (0.121)	22.96 (0.11)	22.09 (0.26)
248	140.59	689.67	21.340 (0.007)	19.541 (0.007)	18.36 (0.01)	17.59 (0.01)
...						

Table 3. Combined WFPC2 and ISAAC measurements in V, I, J_s and the average K_s magnitude of all the stars in AM 1343-452 without extinction correction. For each magnitude in parenthesis we give magnitude errors as given by photometric package, HSTphot and DAOPHOT. Here we give only the first three entries, and the complete table is available through the CDS.

ID	X(WF3)	Y(WF3)	$V(\pm\sigma)$	$I(\pm\sigma)$	$J_s(\pm\sigma)$	$K_s(\pm\sigma)$
825	363.97	755.06	26.114 (0.157)	24.365 (0.133)	23.06 (0.14)	21.86 (0.13)
877	425.34	758.28	23.315 (0.023)	20.553 (0.012)	18.73 (0.01)	17.90 (0.01)
890	219.26	627.35	26.636 (0.194)	23.776 (0.081)	22.49 (0.10)	21.36 (0.09)
...						

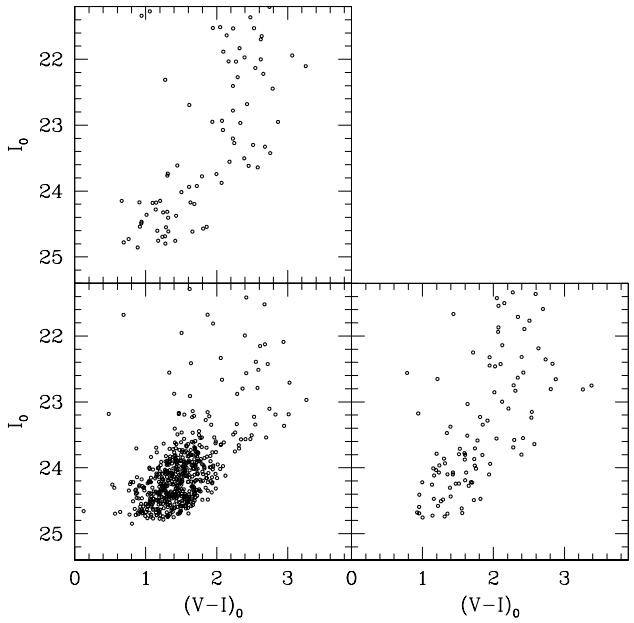

Fig. 4. Reddening corrected CMDs for AM 1343-452 from the WFPC2 data. WF2 is the upper-left, WF3 is the lower-left and WF4 is the lower-right.

Figs. 5 and 6. Consequently, we have decided to match only the WF3 *VI* photometry with the ISAAC data.

The initial coordinate transformations between the WF3 and ISAAC images were calculated using the IRAF tasks *geomap* and *geoxytran*. The transformations were then refined and the combined catalogues made using the DAOMASTER programme (Stetson 1987). The final optical-near-IR photometry lists contain 277 and 190 stars in AM 1339-445 and AM 1343-452, respectively. The complete tables of all the matched sources are published in the electronic version of the paper and are available through CDS. We show in Tables 2 and 3 the photometry for the first three stars in both galaxies.

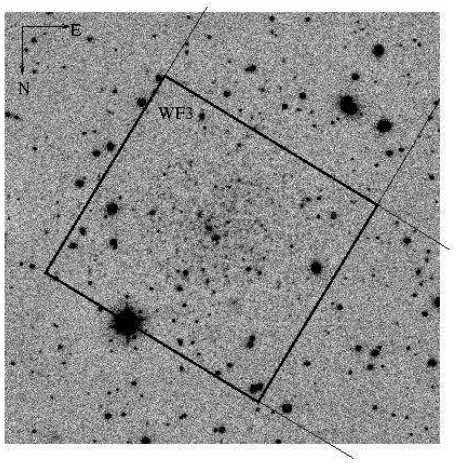

Fig. 5. The ISAAC K-band image of AM 1339-445 taken on May 10, 2004, with the WF3 field of view indicated with thick lines. The thinner lines indicate the overlap with the WF2 and WF4 chips. Seeing measured on this ISAAC image is 0.″50.

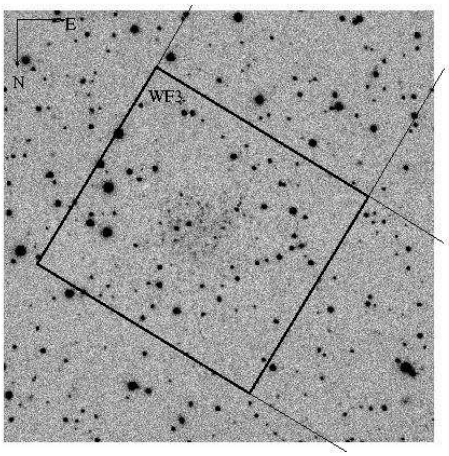

Fig. 6. The ISAAC K-band image of AM 1343-452 taken on June 27, 2004, with the WF3 field of view indicated with thick lines. The thinner lines indicate the overlap with the WF2 and WF4 chips. Seeing measured on this ISAAC image is 0.″58.

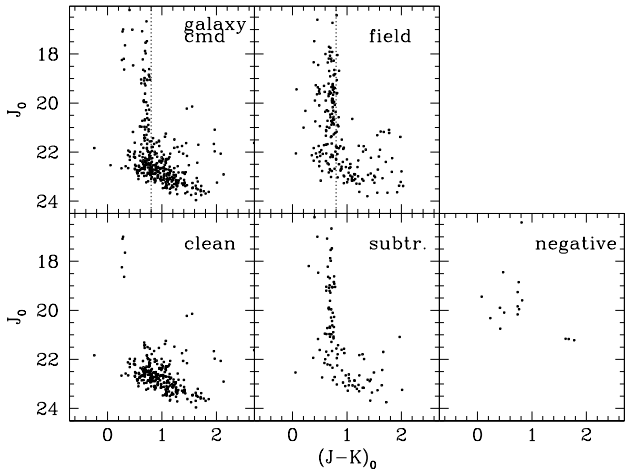

Fig. 7. Decontamination of the CMD for AM 1343-452. In the upper panels are the observed CMDs for the galaxy (left) and field (center) areas. In the bottom panels from left to right there are: the cleaned galaxy CMD (clean), the CMD made of stars subtracted statistically from the galaxy area that had colours and magnitudes similar to those from the field area (subtracted), and the CMD for stars from the field area that had no counterpart in the galaxy area (negative).

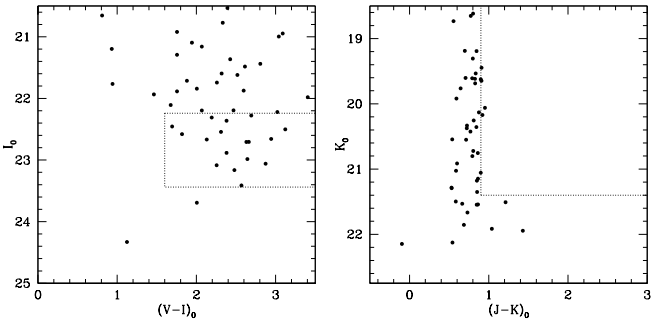

Fig. 8. Example of one simulation of the expected Milky Way foreground stars in the field of view of our combined dataset for AM 1339-445 from the Galaxy model of the Besançon group (Robin et al. 2003). The magnitudes of simulated stars include realistic errors and correction for incompleteness. The dotted lines indicate the boxes used to search for upper-AGB star candidates.

3. Analysis

3.1. Foreground contamination

As is evident in Figs. 1 and 2, the relatively low galactic latitude of the dE fields results in a relatively large number of foreground Galactic stars contaminating the CMDs. The Milky Way's old disk turn-off stars populate the vertical sequence around $(J-K)_0 \simeq 0.35$, fainter red giant branch and red clump stars are found along the most populated sequence at $(J-K)_0 \simeq 0.65$, and the low mass dwarfs with M $\lesssim 0.6\ M_\odot$ have $(J-K)_0 \simeq 0.9$ (Marigo et al. 2003). It is possible also that there are a few contaminating background compact galaxies. However, almost all the foreground stars are have colours bluer than $(J-K)_0 < 0.9$, and in the near-IR CMDs they are well separated from most of the cool giants belonging to the galaxy.

In order to decontaminate the near-IR CMDs we proceeded as follows. First, we determine the galaxy and the field areas on the ISAAC array. The former corresponds to the area where most of the stars would belong to the target galaxy, while the latter contains mostly foreground stars or compact background objects. The stellar radial density distribution was obtained by counting stars in concentric rings centered on the galaxy. The galaxy region was assumed to extend inwards from the level where the stellar density reached 20% of the maximum, while for the field region, we selected the area outwards from the point where the density is 10% of the central value. While it is possible that some galaxy stars are present in the field area, their contribution should be small.

Taking into account the relative sizes of galaxy and field areas, we then subtracted, for each star found in the field area, a star with similar colour and magnitude in the galaxy area. The maximum allowed difference in colour between the two stars takes into account the photometric errors, while the maximum allowed difference in magnitude could be larger to allow for statistical fluctuations in the luminosity distribution of the field stars. The subtraction of a star in the galaxy area depends on whether there is a star with similar colour and magnitude in the field area, and the probability of its subtraction is proportional

to the ratio of galaxy and field areas. We cannot know which stars really belong to galaxy and which to field and thus this decontamination process is necessarily not unique. However, the main features of the subtracted CMDs are robust with respect to different runs of the subtraction code. An example of the decontamination process is shown in Fig. 7 for AM 1343-452. In the upper panels we plot the observed CMDs for the galaxy (left) and field (center) areas. In the bottom panels we plot from left to right: the cleaned galaxy CMD (clean), the CMD made of stars subtracted statistically from the galaxy area that had colours and magnitudes similar to those from the field area (subtracted), and finally on the right the colours and magnitudes of stars from the field area that had no counterpart in the galaxy area (negative). The occurrence of the "negative stars" is not unexpected given likely statistical fluctuations in the colour and magnitude distribution of the stars in the field region.

In the optical, thanks to the orientation of the HST field of view (see e.g. Fig. 5 and 6), larger areas at larger distances from the galaxy centres could be used to estimate the field contamination. For AM 1339-445 the field area is generated from the stars that lie in the halves of the WF2 and WF4 chips furthest from WF3, while for AM 1343-452 it is generated by averaging the numbers of stars on the WF2 and WF4 chips.

Unfortunately, because of the different fields-of-view, a similar procedure could not be employed to decontaminate the combined optical-IR diagrams. However, simulations of the Galactic foreground, using the Besançon group model (Robin et al. 2003), can be used to estimate the possible contamination of the region of the CMDs where upper-AGB candidates are expected to be found. An example of a simulation is shown in Fig. 8, where we note that we have added the simulated stars into our images and remeasured them in order to include realistic errors and incompleteness.

3.2. Near-IR CMDs and luminosity functions

The statistically foreground and background decontaminated near-IR CMDs for both galaxies are shown in Fig. 9. Due to larger size of the galaxy, and consequently smaller field area, the statistical decontamination worked less well in the case of AM 1339-445 leaving a plume of blue stars above the tip of the RGB. Overplotted on these CMDs are the RGB fiducials for Galactic globular clusters from the work of Ferraro et al. (2000), which have been adjusted to the distance modulus adopted for each galaxy (see Sect. 3.3). The giant branches shown extend in metallicity from [Fe/H] = −2.2 to [Fe/H] = −0.2. The large range of $(J-K)_0$ colours along the RGBs of these dE galaxies is almost entirely due to the photometric errors. Unfortunately, incompleteness of around 50% at magnitude $M_K = -5.5$ prevents us from determining reliably the average metallicity from these CMDs. We can only say that the average colour is not inconsistent with the mean metallicity calculated from the optical data.

In both galaxies only the brightest red giants are resolved. The field contamination subtracted and completeness corrected luminosity functions (LFs) for these bright giants are plotted in Fig. 10. For both galaxies the short thick arrow indicates the expected location of tip of the RGB, calculated using the equations (7) and (9) from Valenti et al. (2004) and the distance moduli and mean abundances derived from the optical data in the following section. For AM 1339-445 the expected RGB tip magnitudes are $J_{0,TRGB} = 22.43 \pm 0.21$ and $K_{0,TRGB} = 21.44 \pm 0.23$, while for AM 1343-452 they are

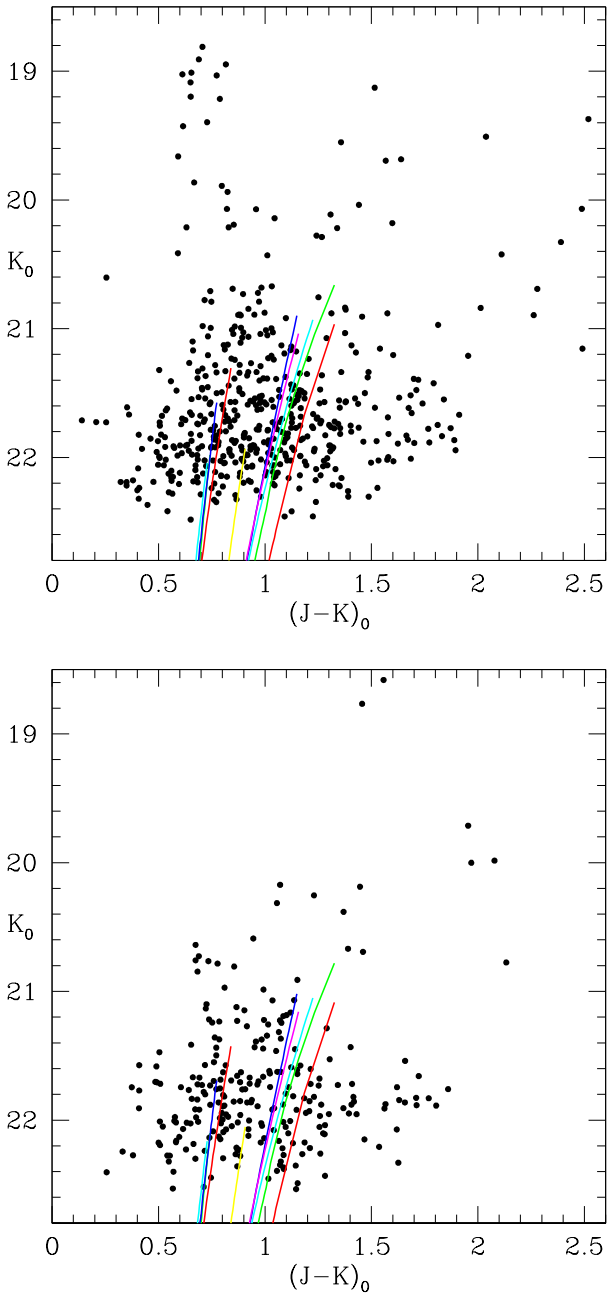

Fig. 9. ISAAC *JK* "cleaned" CMDs for AM 1339-445 (top panel) and AM 1343-452 (bottom) with overplotted fiducial red giant branches for the Galactic globular clusters M15 ([Fe/H] = −2.17), M30 (−2.13), M55 (−1.81), M4 (−1.33), M107 (−0.99), 47 Tuc (−0.71), M69 (−0.59), NGC 6553 (−0.29), and NGC 6528 (−0.23) from Ferraro et al. (2000), corrected for the appropriate distance moduli and reddening, and shown from blue to red.

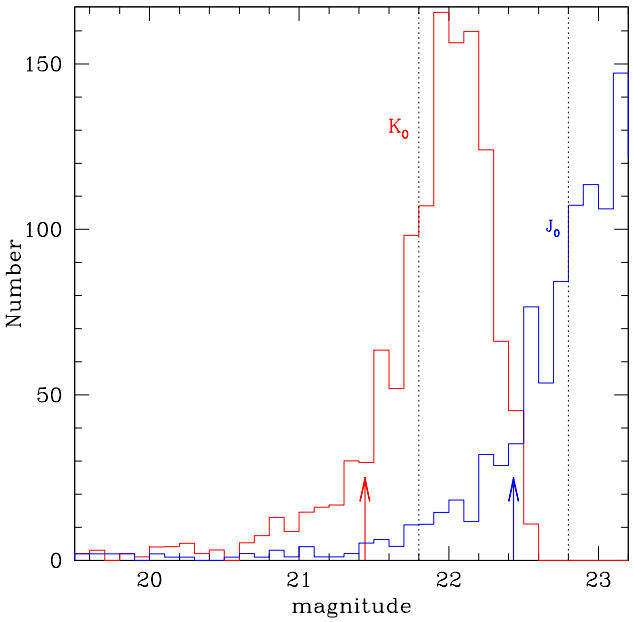

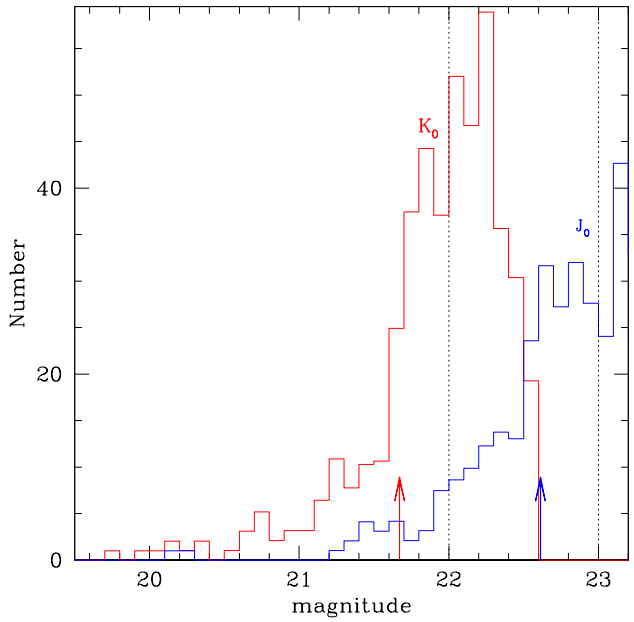

Fig. 10. Completeness corrected and field contamination subtracted J_0 and K_0 luminosity functions for AM 1339-445 (top panel) and AM 1343-452 (bottom panel). Dotted vertical lines indicate 50% completeness limits, while the thick arrows show the expected magnitudes of the RGB tip in the two bands. For AM 1339-445 these are $J_{0,TRGB}$ = 22.43 and $K_{0,TRGB}$ = 21.44, while for AM 1343-452 they are $J_{0,TRGB}$ = 22.61 and $K_{0,TRGB}$ = 21.67.

$J_{0,TRGB} = 22.61 \pm 0.21$ and $K_{0,TRGB} = 21.67 \pm 0.23$. The 50% incompleteness limit, plotted with dotted vertical lines, for both near-IR bands is only few tenths of a magnitude fainter than these expected RGB tip magnitudes, yet the LFs for both galaxies do show the expected rise at or near the predicted RGB tip magnitudes, indicating consistency with the optical results.

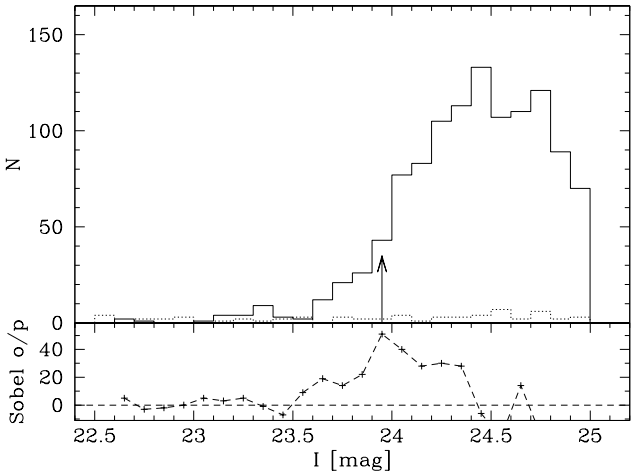

Fig. 11. Top panel: field subtracted (solid line) and field (dotted line) *I*-band luminosity functions for AM 1339-445. Bottom panel: output of a Sobel filter applied to the field subtracted function.

In both galaxies, however, there are a small number of stars above the RGB tip that could belong to an intermediate-age AGB population. We investigate this possibility in more detail in Sect. 3.4 but we note here that at $K_0 \approx 21.3$ and $J_0 \approx 22.3$, the magnitude errors are ±0.18 and ±0.19, respectively for AM 1339-445, while the photometric errors for AM 1343-452 are few hundredths of magnitude smaller. Thus it is unlikely that this excess of stars above the RGB-tip results entirely from magnitude errors for stars at the RGB-tip.

3.3. Optical CMDs and luminosity functions

Figures 11 and 12 show the *I*-band LFs for AM 1339-445 and AM 1343-452, respectively. In the upper panel of each figure, the dotted line shows the field LF. In both cases it is possible that there are some galaxy stars in these adopted field regions, but their numbers are likely to be small. The solid curves in the upper panels of the figures then show the field subtracted LFs for the stars on the WF3 chips. In both cases the field subtracted LFs hover around zero at brighter magnitudes indicating that the adopted field LFs are not grossly in error.

A sharp increase in the number of stars in the LFs is expected at the RGB tip, and to aid in the identification of that feature, we show in the lower panels of the Figures the output of a Sobel edge-detection filter applied to the LF in the upper panels. We adopt the peak in this function as outlining the location of the RGB tip. For AM 1339-445 this results in $I_{TRGB} = 23.95 \pm 0.15$ while for AM 1343-452 we adopt $I_{TRGB} = 24.10 \pm 0.15$, where in each case the uncertainty represents the combination of uncertainty in the peak location, taken as ±0.10 mag (the bin width), and in the photometry zeropoint. These values agree very well with 23.93 ± 0.22 and 24.11 ± 0.25, respectively, listed by Karachentsev et al. (2002).

Da Costa & Armandroff (1990) give a calibration (their equation 3) of the bolometric magnitude of the tip of the red giant branch based on the distance scale of Lee et al.

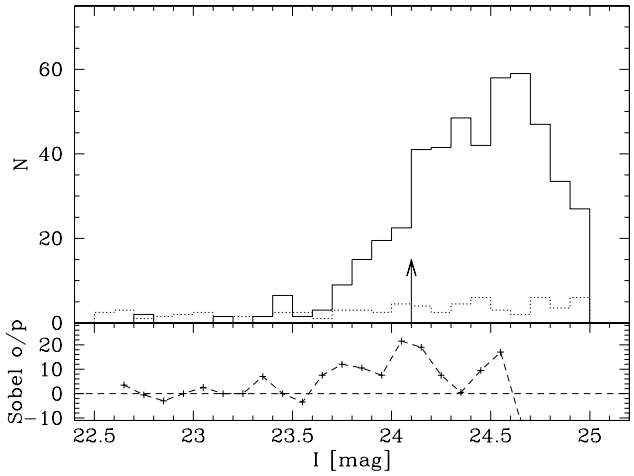

Fig. 12. Top panel: field subtracted (solid line) and field (dotted line) *I*-band luminosity functions for AM 1343-452. Bottom panel: output of a Sobel filter applied to the field subtracted function.

(1990), which includes a dependence on abundance [Fe/H]. Da Costa & Armandroff (1990) also give a relation (their equation 2) for the bolometric correction to the *I* magnitude for red giants as function of $(V-I)_0$ colour. Together these relations yield a calibration of the absolute *I* magnitude of the RGB tip, M_I(TRGB), as a function of [Fe/H] and the dereddened $(V-I)$ colour of the RGB tip. Similarly, Caldwell et al. (1998, see also Armandroff et al. (1993)) give a calibration of abundance [Fe/H], on the Zinn & West (1984) scale, with $(V-I)_{0,-3.5}$, the dereddened colour of the RGB at $M_I = -3.5$. Together these two relations allow the calculation of the mean abundance and distance modulus for each of the galaxies, given *I*(TRGB), $(V-I)$(TRGB) and the reddening.

Using the *I*(TRGB) values given above, the reddening values given in Sect. 2 and $(V-I)_{0,TRGB}$ values from the CMDs shown in Figs. 3 and 4 (the values adopted were 1.70 ± 0.03 and 1.59 ± 0.03, respectively), we derive distance moduli for the two galaxies as $(m-M)_0$(AM1339 − 445) = 27.74 ± 0.20, and $(m-M)_0$(AM1343 − 452) = 27.86 ± 0.20. The uncertainties listed take into account uncertainties in the zeropoints of the photometry, the uncertainty in the derived mean abundances and the uncertainty in the location of the RGB tip. These values are again very similar to the distance moduli determined by Karachentsev et al. (2002), who give slightly larger values (27.77 ± 0.21 for AM 1339-445, and 27.92 ± 0.25 for AM 1343-452) resulting from their use of a slightly brighter value for M_I(TRGB). They are also in very good agreement with measured distances from surface brightness fluctuation method by Jerjen et al. (2000b), who list distances corresponding to moduli of 27.87 ± 0.27 for AM 1339-445 and 27.99 ± 0.37 for AM 1343-452.

The mean metallicities of the two galaxies, as determined from the mean colour of the RGBs in a ±0.1 mag interval in *I* about $M_I = -3.5$, are ⟨[Fe/H]⟩ = −1.4 ± 0.2 for AM 1339-445 and ⟨[Fe/H]⟩ = −1.6 ± 0.2 for AM 1343-452. The listed uncertainty here includes the effect of uncertainty in the distance moduli, the statistical and photometric zeropoint uncertainty, ±0.02 and ±0.03 mag, respectively, and uncertainty in the abundance calibration. These four contributions are all approximately equal in size and have been added in quadrature to determine the overall uncertainty. In Fig. 13 we show the WF3 photometry for each galaxy with the giant branches of standard globular clusters from Da Costa & Armandroff (1990) overplotted, using the distance moduli derived above. The four clusters are M15 ([Fe/H] = −2.17), M2 (−1.62), NGC 1851 (−1.36) and 47 Tuc (−0.71). We also note that, due to the limited exposure times and the consequent size of the errors in the colours for the individual RGB stars, it is not possible to place any meaningful constraints on the size of any metallicity spread in these galaxies.

Strictly speaking the average metallicity derived in this way is only valid for stellar populations with an age comparable to that of Galactic globular clusters. Saviane et al. (2000) discuss the effect of the younger mean age of the population and the RGB colour in Fornax dE. They find that the bluer colours of the 5 Gyr old population mimic a ∼ 0.4 dex more metal-poor stellar population of 15 Gyr. Later we will argue that a significant intermediate-age population is present in our targets, although with a much lower fraction than in Fornax. Hence we estimate that our average metallicities might be systematically too low by up to ∼ 0.2 dex. Fortunately, none of the conclusions in the following sections are significantly altered if the true metallicities exceed those listed by amounts of this order. A more detailed discussion of the influence of the composite stellar populations on the photometric metallicities and on the measurement of distances via RGB tip method is available in Salaris & Girardi (2005).

In general, the optical CMDs (Fig. 13) are consistent with the old metal-poor population expected for dE galaxies. They are dominated by red giants and there is no indication of any (young) blue stars. The relatively low Galactic latitude of the fields, however, results in significant contamination of the CMDs by foreground Galactic stars, particularly for magnitudes above the red giant branch tip. Most of them are field red clump stars that have optical colours similar to metal-poor RGB and AGB stars. Identification of any upper-AGB stars is therefore not as straightforward as it is for dEs in higher latitude fields (cf. Caldwell et al. 1998).

The LFs in Figs. 11 and 12 clearly show an apparent excess of stars above the field LFs at luminosities above that of the RGB tip. At the tip of the RGB, the typical error in the *I* magnitudes is $\sigma(I) \approx 0.1$ mag. Consequently, given that any star whose photometry was affected by crowding by more than 0.05 mag has been excluded, it is entirely plausible that these stars, particularly those more than 0.2-0.3 mag above the RGB tip, are indeed intermediate-age upper-AGB stars. We now use our combined optical/near-IR dataset to investigate this possibility.

3.4. Candidate upper-AGB stars

Asymptotic giant branch stars (AGB) brighter than the RGB tip are found in relatively metal-poor intermediate-age popula-

Table 4. Dereddened magnitudes in V, I, J_s and the two measurements in the K_s filter of AGB star candidates. In the last two columns we list absolute bolometric magnitudes of these stars calculated using the appropriate distance modulus and $[BC_{I_c}, (V-I)_c]$ relation of Da Costa & Armandroff (1990), and $[BC_K, (J-K)]$ of Costa & Frogel (1996), in columns 9 and 10, respectively.

ID	X(WF3)	Y(WF3)	$V_0(\pm\sigma)$	$I_0(\pm\sigma)$	$J_0(\pm\sigma)$	$K_1(\pm\sigma)$	$K_2(\pm\sigma)$	$M_{bol}(VI)$	$M_{bol}(JK)$
AM 1339-445									
560	352.55	527.38	25.591 (0.109)	23.236 (0.066)	22.35 (0.08)	21.00 (0.09)	21.21 (0.16)	−4.20	−3.75
684	367.45	444.05	25.186 (0.083)	23.402 (0.070)	21.87 (0.06)	20.93 (0.10)	20.84 (0.07)	−3.89	−4.24
720	325.04	378.23	24.904 (0.066)	22.933 (0.051)	21.70 (0.05)	20.73 (0.08)	20.61 (0.07)	−4.41	−4.40
729	119.52	194.34	25.361 (0.084)	23.047 (0.053)	21.76 (0.06)	20.82 (0.09)	20.73 (0.11)	−4.38	−4.35
780	499.28	480.96	24.981 (0.072)	23.303 (0.073)	22.27 (0.09)	21.28 (0.13)	21.31 (0.15)	−3.97	−3.84
812	130.06	140.34	24.796 (0.059)	22.955 (0.050)	21.51 (0.05)	20.41 (0.07)	20.30 (0.07)	−4.36	−4.58
817	576.48	522.78	24.981 (0.075)	23.130 (0.059)	21.44 (0.04)	20.48 (0.06)	20.34 (0.07)	−4.18	−4.67
857	351.16	300.80	25.033 (0.071)	23.139 (0.060)	21.78 (0.06)	20.20 (0.05)	20.16 (0.05)	−4.19	−4.39
1046	501.73	276.17	24.904 (0.075)	23.093 (0.057)	21.52 (0.05)	20.28 (0.06)	20.27 (0.06)	−4.21	−4.57
1087	389.85	153.30	25.297 (0.084)	23.256 (0.062)	22.21 (0.08)	20.81 (0.08)	20.92 (0.15)	−4.10	−3.90
1114	761.45	447.66	25.019 (0.073)	23.311 (0.066)	22.35 (0.09)	21.21 (0.12)	20.92 (0.09)	−3.96	−3.74
AM 1343-452									
890	219.26	627.35	26.237 (0.194)	23.540 (0.081)	22.38 (0.10)	21.40 (0.14)	21.22 (0.13)	−4.10	−3.84
982	409.25	691.57	25.318 (0.095)	23.547 (0.084)	22.39 (0.08)	21.35 (0.14)	21.52 (0.16)	−3.87	−3.86
1042	485.46	695.75	26.020 (0.157)	23.191 (0.062)	21.37 (0.04)	20.27 (0.05)	20.35 (0.05)	−4.48	−4.85
1197	581.90	657.49	25.999 (0.160)	23.506 (0.080)	22.06 (0.08)	20.62 (0.05)	20.79 (0.08)	−4.09	−4.17
1232	484.85	583.75	24.536 (0.057)	22.911 (0.054)	22.43 (0.12)	20.71 (0.06)	20.90 (0.08)	−4.47	−3.88
1484	350.15	394.85	25.113 (0.084)	23.218 (0.067)	21.97 (0.11)	20.34 (0.07)	19.98 (0.04)	−4.23	−4.52
1526	342.88	370.90	25.270 (0.093)	23.346 (0.073)	21.53 (0.05)	20.63 (0.06)	20.34 (0.06)	−4.11	−4.71
1542	356.72	373.95	25.619 (0.135)	23.336 (0.072)	21.75 (0.07)	20.88 (0.10)	20.72 (0.09)	−4.21	−4.49
1587	314.38	326.92	25.161 (0.082)	22.797 (0.049)	21.79 (0.05)	20.49 (0.06)	20.53 (0.06)	−4.76	−4.42
1572	293.25	322.81	25.317 (0.100)	23.765 (0.096)	22.22 (0.08)	21.29 (0.10)	20.81 (0.09)	−3.59	−4.01

tions, and in metal-rich ([Fe/H] $\gtrsim -1$ dex) and old systems (Frogel & Whitelock 1998; Guarnieri et al. 1998). In metal-poor old Galactic globular clusters, stars brighter than the RGB tip are not observed, while they are present in the intermediate-age LMC and SMC clusters (Frogel et al. 1990). Since the estimated average metallicity of our target galaxies shows that they are relatively poor in metals, any bright AGB stars above the tip of the RGB are expected to belong to an intermediate-age population. Due to their cool atmospheres these stars are particularly bright in the near-IR wavelength range. Moreover, they are typically redder than Galactic foreground stars, and thus relatively easy to detect. In optical CMDs, however, this distinction is less easy. The availability of matched optical and near-IR photometry allows us to investigate the presence or absence of bright AGB stars in our target galaxies.

In Sect. 2.3 we described the combination of the optical and near-IR datasets to produce a sample of stars in both galaxies with *VI* and *JK* photometry. The CMDs for these combined datasets are shown in Figures 14 and 15 for AM 1339-445 and AM 1343-452, respectively. We have adopted the following criteria to identify candidate upper-AGB stars in these diagrams. First, in the near-IR CMDs we insist that any upper-AGB star candidate be redder than the field sequence and be brighter than the RGB tip. In other words, the candidates must satisfy $(J-K)_0 > 0.90$ and $K_0 < 21.4$ (AM 1339-445) or $K_0 < 21.7$ (AM 1343-452). These boundaries are shown as the dotted lines in the *JK* CMDs. To place similar limits in the *VI* CMDs we use as guide the HST WFPC2 imaging of two M81 group dEs discussed in Caldwell et al. (1998). Although the two dwarfs studied, F8D1 and BK 5N, are at a comparable distance to the dEs studied here, the considerably longer total exposure times and the comparatively high Galactic latitude of the M81 group, results in precise CMDs that are essentially free of foreground and background contamination. Both these M81 group dEs show clear upper-AGB populations (Caldwell et al. 1998), and we use these populations to guide our selection of candidates in the *VI* CMDs for the Cen A group dEs. We note that the upper-AGB populations occupy a region in the M81 group dEs corresponding to $1.6 \leq (V-I)_0 \leq 3.3$ and $-4.3 \geq M_I \geq -5.5$. Here the fainter limit has been specifically chosen to exceed the RGB tip magnitude by ∼0.3 to minimise, for the Cen A group dEs where the uncertainties are larger, the possibility of false candidates arising from RGB tip stars displaced upwards by photometry errors. This selection region is outlined by the dotted-line rectangles in the *VI* CMDs.

The stars that satisfy the criteria for candidate upper-AGB stars in *both* the *VI* and *JK* CMDs are plotted with filled symbols in Figures 14 and 15. There are 11 such stars in AM 1339-445 and 9 in AM 1343-452. The two long period variable star candidates in AM 1343-452 (#1484 and #1526; see below) that satisfy both selection criteria in *VI* and *JK* CMDs are plotted with filled (blue) squares. In addition, one star with an *I* magnitude only slightly brighter than the RGB tip (#1572; shown with large filled (green) triangle in the CMDs), and thus fainter than our conservative limit set to 0.3 mag brighter than the RGB tip in the *I* filter, was included in the list of candidate AGB stars in AM 1343-452 as it is also a potential long period variable star. The full set of photometry measures for these candidate upper-AGB stars are given in Table 4.

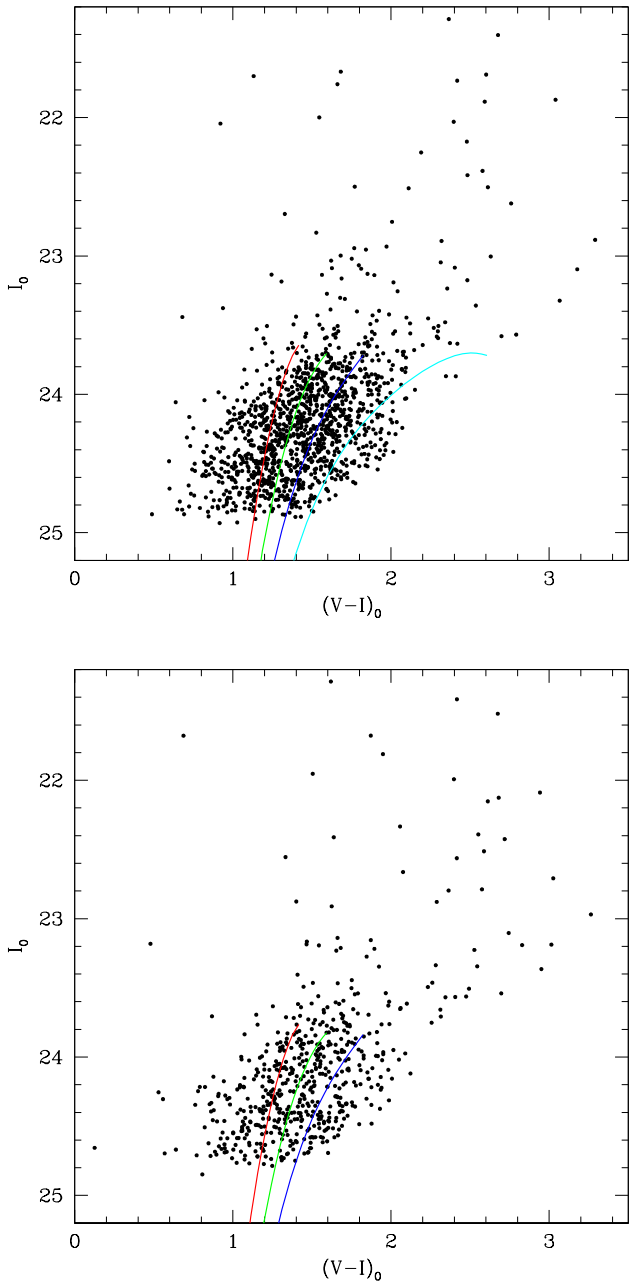

Fig. 13. WF3 *VI* CMDs for AM 1339-445 (top panel) and AM 1343-452 (bottom panel) with fiducial red giant branch for the Galactic globular clusters M15 ([Fe/H] = −2.17), M2 (−1.62), NGC 1851 (−1.36) and 47 Tuc (−0.71) overplotted, using the appropriate distance moduli and reddening. The 47 Tuc giant branch is not plotted for AM 1343-452.

In Fig. 16 we show $(V-K)_0$ vs. K_0 CMDs for both galaxies with RGB fiducials for Galactic globular clusters M15([Fe/H] = −2.17), M30 (−2.13), M55 (−1.81), M4 (−1.33), M107 (−0.99) and 47 Tuc (−0.71) from Ferraro et al. (2000) overplotted using the appropriate distance moduli and reddening. As can be seen by the wide spread in colour of these globular cluster RGB fiducials, $(V-K)_0$ colour is particularly sensitive to metallicity. The $(V-K)_0$ colours of the red giants

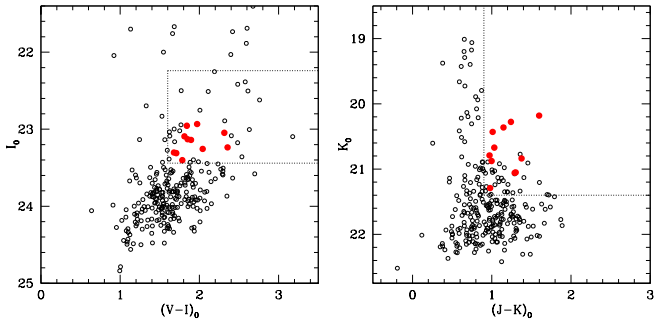

Fig. 14. *VI* and *JK* CMDs of AM 1339-445 with adopted box for the selection of upper-AGB candidates. All the candidate upper-AGB stars are plotted with large filled symbols.

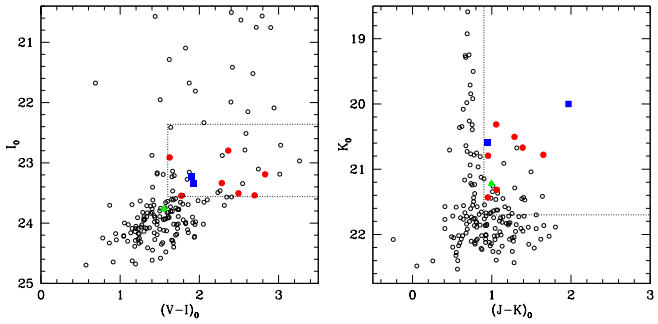

Fig. 15. *VI* and *JK* CMDs of AM 1343-452 with adopted box for the selection of upper-AGB candidates. All the candidate upper-AGB stars are plotted with large filled symbols. The three candidate long period variable stars are plotted as large (blue) squares and a (green) triangle.

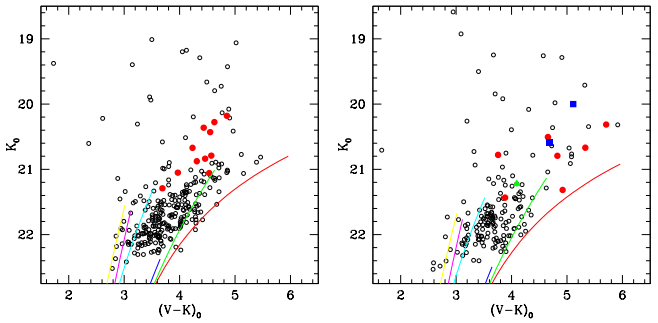

Fig. 16. *VK* CMDs for the stars found in common in HST WF3 and ISAAC J_s and K_s images for AM 1339-445 (left panel) and AM 1343-452 (right panel). The lines are Galactic globular cluster RGB fiducials for M15([Fe/H] = −2.17), M30 (−2.13), M55 (−1.81), M4 (−1.33), M107 (−0.99) and 47 Tuc (−0.71) from Ferraro et al. (2000), plotted using the appropriate distance moduli and reddening, and going from blue to red. The large filled symbols show the position of upper-AGB star candidates in these two galaxies. The two candidate LPVs in AM 1343-452 that are located within the selection boxes in Fig. 15 are plotted with filled (blue) squares and the additional LPV candidate with slightly fainter *I*-band magnitude than our selection limit is plotted with a (green) triangle.

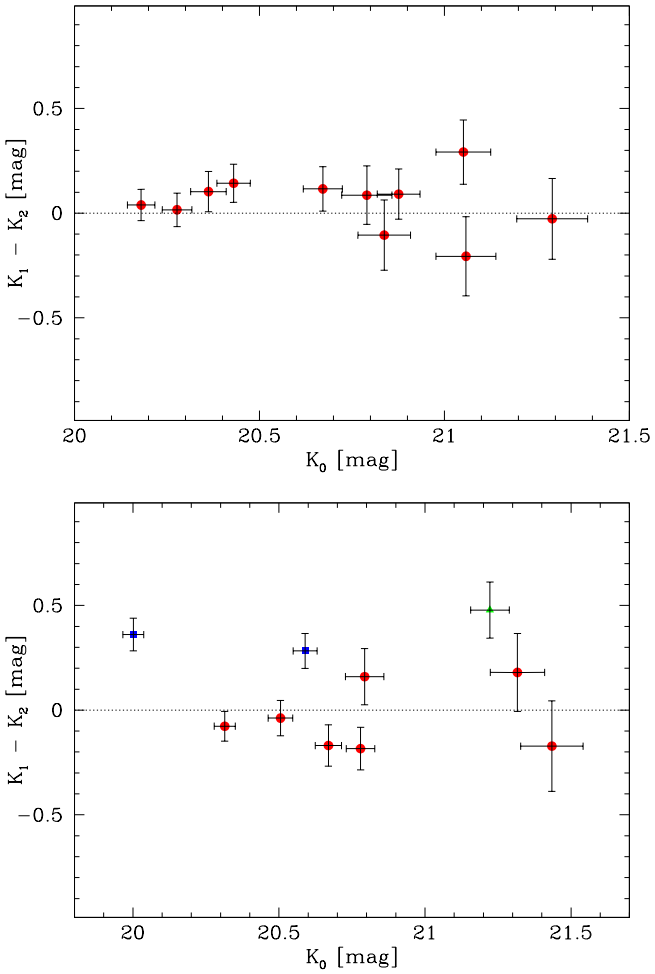

Fig. 17. Top panel: *K*-band magnitude difference measured between the two epochs for the upper-AGB star candidates in AM 1339-445. Due to the only 4 day interval between the two observations, none of the stars displays any variability. Bottom panel: *K*-band magnitude difference measured between the two epochs for the upper-AGB star candidates in AM 1343-452. The time interval between the two epochs is 43 days. Three of the stars, plotted as filled (blue) squares and filled (green) triangle (see text), are LPV candidates as their magnitudes vary by more than 0.25 mag and the difference is more than 3.3 σ larger than the combined photometric errors.

in these two galaxies are bracketed by M55 and M107 ridge lines as expected from the average metallicity derived from the optical data alone. The AGB candidates are plotted with larger filled symbols and are seen to have magnitudes brighter than the RGB tip and relatively red $(V-K)$ colours. This is further confirmation that these stars are plausible upper-AGB candidates.

We also searched for stars with very red $(J_s - K_s)$ colours, stars that are well measured on both K images but which have no counterpart on the J-band image. Such stars might be dust enshrouded AGB stars, similar to those present in Leo I (Menzies et al. 2002) and F8D1 (Da Costa 2004). Two such very red stellar objects are indeed present in AM 1343-452,

Table 5. K-band photometry and positions of two very red objects in field of AM 1343-452.

ID	α_{2000}	δ_{2000}	$K_1(\pm\sigma)$	$K_2(\pm\sigma)$
1182	13:46:13	−45:41:27	21.09 (0.11)	21.12 (0.12)
2040	13:46:15	−45:40:52	20.81 (0.10)	20.61 (0.08)

while none were found in AM 1339-445. Neither of the two very red stars in AM 1343-452 show significant variability between the two K magnitude measurements. One star (#2040) is within the field of view of WF3 chip of WFPC2, but is not detected in the F814W image. The second red object (#1182) is found well outside the main body of the galaxy, and just outside of the WFPC2 field of view. While it is possible that that object is a compact high redshift galaxy, it is also not excluded that it belongs to AM 1343-452. For example, in Leo I one of the five very red stars is also found well away from the center of its host galaxy (Menzies et al. 2002). The photometry and positions of the two very red stars in the field of AM 1343-452 are listed in Table 5. Given that for these stars J_0 exceeds 23, the 50% completeness limit, they must have $(J-K)_0 \geq 1.9$ and 2.3, respectively.

A distinguishing characteristic of upper-AGB stars is that most, if not all, are long period variables (LPV) displaying large amplitude variations, particularly at optical wavelengths (e.g. Whitelock et al. 2000). For example, a large fraction of the upper-AGB stars identified by Caldwell et al. (1998) in the M81 group dEs are evidently variables (Caldwell et al. 1998). As the name implies, the periods for the variability are long, typically hundreds of days. These amplitude and period properties make such stars relatively easy to detect, given sufficient epochs, from the ground even in crowded fields and at distances of 4 Mpc or larger (Rejkuba et al. 2003). Variability is thus a further criterion against which we can assess our candidate upper-AGB stars. Unfortunately, due to an operational oversight, the two *K*-band epochs for AM 1339-445 were observed only 4 days apart. This is much smaller than the variability timescale of LPVs and thus it is not surprising that none of the upper-AGB candidates display variability (Fig. 17 top panel). On the other hand, the AM 1343-452 *K*-band observations are separated by 43 days. Of course, with just two epochs we can only set a lower limit to the number of variables, as some may change very little in the interval or be caught at two phases that have similar brightnesses. Nevertheless it is encouraging to see in the bottom panel of Fig. 17, where we plot $\Delta K = K_1 - K_2$, the *K*-band magnitude difference measured between the two epochs for the AM 1343-452 upper-AGB star candidates, that two of these stars, #1484 and #1526 (filled blue squares), are indeed probable variables. In both cases the magnitude difference is more than 3.3 σ larger than the combined photometric errors of the two measurements. This result suggests that we are indeed selecting genuine candidate upper-AGB stars. Based on such variability criteria, we add one more star, #1572, to the list of upper-AGB candidates. This one has *I* magnitude of 23.77 and it is only very slightly brighter than the RGB tip in AM 1343-452 ($I_{0,TRGB} = 23.86$), and thus outside our conservative AGB selection box in the *VI* CMD, while it is within

the AGB selection box in the *JK* CMD. We plot this star with filled (green) triangle in both panels in Fig. 15. With this star and the two very red objects, our final upper-AGB candidate list for AM 1343-452 contains a total of 12 stars, while that for AM 1339-445 remains at 11. We will discuss the characteristics of these stars and the implications they provide for the star formation histories of the dEs in Sect. 4.

3.5. Globular Clusters

Sharina et al. (2005) made a search for globular cluster candidates in low surface brightness dwarf galaxies, based on WFPC2 HST archival images. In AM 1343-452 they found no globular cluster candidates, but AM 1339-445 has two. Both of them are located on WF3 chip and are present in our ISAAC dataset.

We have measured J_s and K_s magnitudes for these two globular cluster candidates on our ISAAC images and report the reddening corrected J_0 and K_0 magnitudes in Table 6 together with optical magnitudes published by Sharina et al. (2005). We compare the colours of these candidates, plotted as filled symbols with error-bars, with those of the Milky Way (open circles; Aaronson, Malkan & Cohen; private communication from J. G. Cohen) and M31 (open triangles; Barmby et al. 2000) globular clusters in Fig. 18. For additional comparison, we also plot the iso-age line for a 12 Gyr single stellar populations (SSP) with metallicities ranging from [Fe/H] = −2.25 to solar from Maraston (1998, 2005) models. The two globular cluster candidates have optical and near-IR colours similar to those of the old and metal-poor globular clusters in these two large spiral galaxies. If we assume that their age is of the order of 12 Gyr, then the AM 1339-445 clusters would have metallicities between $-1.8 \lesssim$ [Fe/H] $\lesssim -1.4$.

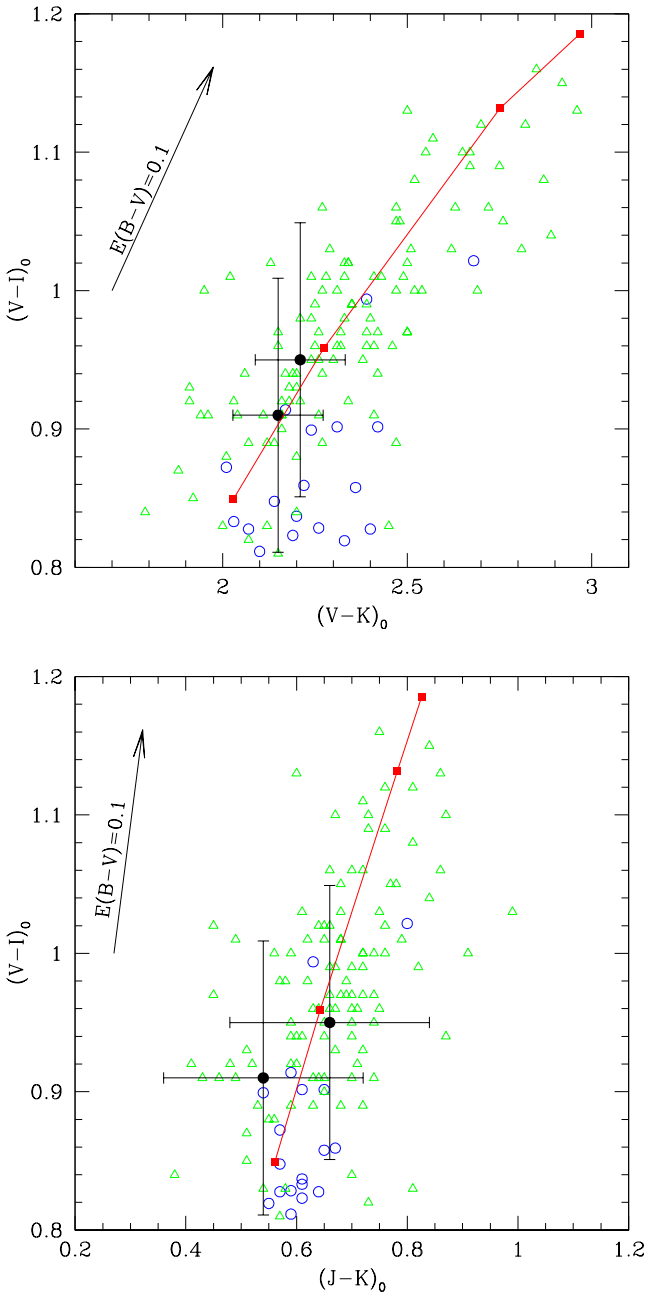

Fig. 18. Comparison of the optical and near-IR colours for the two globular cluster candidates in AM 1339-445 (filled dots with error-bars), selected by Sharina et al. (2005), with globular clusters in the Milky Way (open circles) and M31 (open triangles). We also plot a 12 Gyr constant age line for different metallicities (filled squares): [Fe/H] = −2.25, −1.35, −0.33 and 0.0 dex, going from blue to red colours (Maraston 1998, 2005). The reddening vector is plotted in the upper left for E(B − V) = 0.1 mag.

4. Discussion

Given the distance moduli and reddenings of the previous sections, we can now use the *VI* and *JK* photometry of the upper-AGB candidates given in Table 4 to calculate M_{bol} values for the stars. For the *VI* photometry we adopt the bolometric correction to the *I* magnitude given by equation (2) of Da Costa & Armandroff (1990). Although based on globular cluster red giants, through the inclusion of red luminous giants in 47 Tuc this equation is valid at least to $(V-I)_0 \approx 2.6$. It is thus applicable to all the stars in Table 4 with the exception of the two reddest stars in AM 1343-452. For these stars we have assumed that the relation can be extrapolated. Da Costa & Armandroff (1990) note that there is no obvious metallicity dependance in the adopted equation, and that the dispersion about the fitted relation, 0.06 mag, is consistent with the observational errors. Using this relation, the three[1] most luminous of the AM 1339-445 stars in Table 4 all have $M_{bol} \approx -4.4$, while for AM 1343-452, the most luminous star has $M_{bol} \approx -4.75$ with the two next most luminous stars both having $M_{bol} \approx -4.5$.

For the *JK* photometry, there are a number of possible relations that provide bolometric corrections to the *K* mag as a function of $(J-K)_0$ colour. These include the relations

[1] In the following, wherever the sample of upper-AGB stars is small, we give the luminosity of the three most luminous stars so as to indicate the likely location of the upper-AGB tip, and its uncertainty.

Table 6. Photometry of Globular Cluster Candidates in AM 1339-445. The first three columns are the identifier, and the coordinates of the candidate globular cluster from Sharina et al. (2005). After that we list their (X,Y) positions in the ISAAC J_s band image and integrated apparent V, I, J and K magnitudes (corrected for Galactic extinction using Schlegel et al. (1998) maps) and corresponding errors.

ID	α_{2000}	δ_{2000}	X(ISAAC)	Y(ISAAC)	V_0	I_0	J_0	K_0
KK211–3–917	13:42:08.0	−45:12:29	611.21	500.09	20.91 ± 0.07	20.00 ± 0.07	19.3 ± 0.15	18.76 ± 0.10
KK211–3–149	13:42:05.6	−45:12:20	435.92	433.74	19.95 ± 0.07	19.00 ± 0.07	18.4 ± 0.15	17.74 ± 0.10

Table 7. Absolute bolometric magnitudes for the brightest upper AGB stars in AM 1339-445 and AM 1343-452 compared with those in the dE companions of the MW and M31. For the MW dE companions we also list the time of the last significant star formation episode. The references to the literature data for the AGB star magnitudes, and for the star formation histories (only for the MW dE companions) are given in columns 3 and 5, respectively.

galaxy	M_{bol}	M_{bol} reference	last SF	SFH reference
AM 1339-445	≈ −4.5	*this work*		
AM 1343-452	≈ −4.8	*this work*		
Leo I	−5.1 to −4.2	Menzies et al. (2002)	1–2 Gyr	Gallart et al. (1999)
Fornax	−5.2, −5.05, −4.8	Demers et al. (2002)	300–400 Myr	Saviane et al. (2000)
Carina	−4.8, −4.7, −4.55	Mould et al. (1982)	∼ 3 Gyr	Hurley-Keller et al. (1998)
Leo II	−4.3, −4.1, −3.9	Aaronson & Mould (1985)	∼ 7 Gyr	Mighell & Rich (1996)
NGC 147	−5.3	Nowotny et al. (2003)		
NGC 185	−5.3	Nowotny et al. (2003); Kang et al. (2005)		
And II	−4.7, −4.5, −4.25	Kerschbaum et al. (2004)		

given by Bessell & Wood (1984), who list relations based on oxygen-rich stars in the LMC and the Galaxy, and on similar stars in 47 Tuc and the SMC. Similarly, Costa & Frogel (1996) give a relation derived from carbon stars in the LMC, while Bergeat et al. (2002) tabulate bolometric corrections as a function of $(J-K)_0$ based observations of Galactic carbon-rich giants. We have investigated these relations and find that, for the colour[2] range of the stars in Table 4, the differences are small (≤0.10 mag) and are essentially independent of colour. This is important because without further information we cannot be certain whether the candidate upper-AGB stars are M stars (oxygen-rich) or C stars (carbon-rich). We note though that in metal-poor galaxies similar to those studied here, stars with $(J-K)_0$ between ∼1.3 – 1.5 and 2 are typically found to be carbon-rich (e.g. Cioni & Habing 2003; Raimondo et al. 2005). In our upper-AGB candidate lists there are 3 stars in each galaxy that fall in this colour range. These stars may well be C stars, although more precise photometry will be needed to be certain of the classification.

For the bolometric corrections to the *JK* photometry we adopt the relation of Costa & Frogel (1996) as it gives corrections that lie between those of Bessell & Wood (1984) and Bergeat et al. (2002). With this relation, the three most luminous stars (now based on the *JK* photometry) in AM 1339-445 all have $M_{bol} \approx -4.6$, while for AM 1343-452 the most luminous star has $M_{bol} \approx -4.85$ with the next two most luminous having $M_{bol} \approx -4.7$ and −4.5.

As noted above, most upper-AGB stars are long period variables. Consequently, given the significant epoch difference between the *VI* and *JK* photometry, we should not necessarily expect the most luminous stars in each set to coincide. Further, given the photometric errors and potential systematic differences between the *VI* and *JK* bolometric corrections, we should also not necessarily expect the luminosities of the brightest star, or any combination of the luminosities of the brighter stars to agree. It is gratifying, therefore, to note that for each galaxy there is a reasonable degree of consistency between the two sets of data. For AM 1339-445 the brightest stars have $M_{bol} \approx -4.5 \pm 0.1$ regardless of whether the single most luminous, or the mean of the 3 most luminous stars, are considered for both the *VI* and *JK* data sets. One star is also common to the most luminous three from the two sets. Similarly, the most luminous AM 1343-452 star in our chosen sample has $M_{bol} \approx -4.8 \pm 0.1$ regardless of which data set is used, and the mean of the three most luminous stars is -4.65 ± 0.1 again independent of the photometry set. As for AM 1339-445, there is one star common to the most luminous three in the two data sets.

We have then our first clear result: *the upper-AGB reaches 0.2 – 0.3 mag brighter in AM 1343-452 than it does in AM 1339-445*. We note, however, that the numbers of upper-AGB candidates are simply too small to assert with any statistical significance (e.g. $\geq 2\sigma$) that there are also relatively more upper-AGB stars in AM 1343-452 than in AM 1339-445, despite the 12 vs 11 candidate ratio and a luminosity ratio for the areas surveyed of approximately 0.48 to 1.00.

How do these luminosities compare with those for upper-AGB stars in other dE galaxies? We give in Table 7 data for the MW dE companions with clearly established upper-AGB populations. For each dE, we list the absolute bolometric magnitudes for the few brightest upper-AGB stars (full range for Leo I) in column 2 with the reference to the literature source

[2] We have adopted the weighted mean of the two *K*-band observations in Table 4 as the *K* magnitude and used that with the *J* magnitude to form the $J-K$ colour.

of the photometry in column 3. In most cases, the exception is Leo I where we have taken the values directly from Menzies et al. (2002), the listed M_{bol} values were obtained from the published photometry assuming distance moduli from Mateo (1998) and the bolometric corrections of Costa & Frogel (1996). We also list in column 4 the time when the last significant star formation episode ceased, based on literature data, referenced in column 5. These epochs are derived from analyses of star formation histories that are based on CMDs reaching well below the main sequence turnoff.

As for the dE companions to M31, the more luminous systems all contain notable populations of upper-AGB stars (e.g. Battinelli & Demers 2004a,b; Demers et al. 2003, and the references therein). In particular, as indicated in Table 7, both NGC 147 and NGC 185 contain stars as bright as $M_{bol} \approx -5.3$ (Nowotny et al. 2003); see also Kang et al. (2005). However, unlike the majority of the MW's dE satellites, the low luminosity dE satellites of M31 generally lack upper-AGB populations, with only And II and And VII (Cas) known to contain such stars (Aaronson et al. 1985; Harbeck et al. 2004). Kerschbaum et al. (2004) identify and give photometry for 7 carbon stars in And II. Using the *VI* bolometric corrections of Da Costa & Armandroff (1990) and distance and reddening values from Da Costa et al. (2000), we give the bolometric magnitudes for the three most luminous of these stars in Table 7. These values are somewhat brighter than those discussed in Sect. 3.5.2 of Da Costa et al. (2000), though it is unclear whether there are any stars in common. No deep CMDs exist for the dE companions of M31, although, with Advanced Camera for Surveys (ACS) on board HST, it is now possible to obtain such data (Brown et al. 2003).

We have then our second result: *the luminosities of the candidate upper-AGB stars found here for the Cen A group dEs AM 1339-445 and AM 1343-452 are clearly quite comparable to those seen among Local Group dEs*.

We turn now to estimating the age of the most luminous of the upper-AGB stars in each dE. The relatively small numbers of stars in our candidate lists, combined with the rapidity of this evolutionary phase, means that the age estimates derived below should strictly be considered upper limits: it is possible that a larger sample (assuming it was possible to generate one) might reveal more luminous stars. For this same reason, the derived ages should be considered as limits on the epoch of the most recent episode of significant star formation in these galaxies: star formation may well have continued past these eras at a sufficiently low rate that the upper-AGB is simply not populated. A further complication is that modeling the thermally-pulsing phase of AGB evolution is difficult to carry out in detail, and the results are sensitive to the mass-loss prescriptions and the details of the mixing processes that occur during the thermal pulses, as well as to changes in molecular opacities during the third dredge-up (Marigo 2002). Thus any theoretical calibration of AGB tip luminosity with age and abundance is necessarily uncertain. The star clusters of the Magellanic Clouds, however, provide a set of objects with which an empirical calibration of the bolometric magnitude of the AGB tip as a function of age can be generated. While these clusters, particularly those in the LMC, are somewhat more metal-rich than the dE

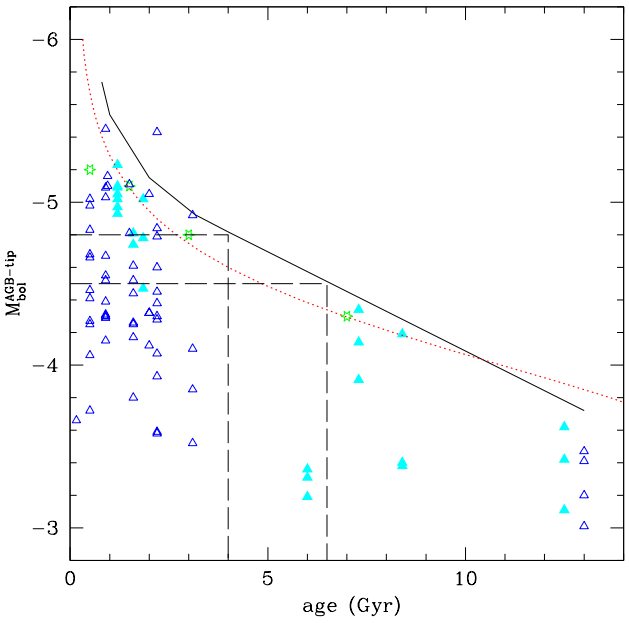

Fig. 19. Our adopted relationship between AGB tip luminosity and age is shown as a solid line. The LMC and SMC cluster data used to constrain this relation are shown as open (blue) triangles and filled (cyan) triangles, respectively. The dotted (red) line shows the theoretical AGB tip luminosity-age relationship from Stephens & Frogel (2002). With open (green) star symbols we plot the MW dE galaxies from Table 7, while dashed lines are used to indicate the measured AGB tip bolometric magnitudes and the inferred ages of the last significant star formation event for the two dEs in Cen A group.

stars considered here, the theoretical models suggest that the dependance on metallicity at fixed age is not large. For example, using the isochrones of Girardi et al. (2002), the difference in AGB tip luminosity at 2 Gyr for metallicities Z=0.0004 and Z=0.004 is only ∼0.3 mag (the more metal-poor brighter), with the difference decreasing with increasing age. Conversely, for the same isochrones, the difference in the AGB tip luminosity between 1 and 3 Gyr is ∼0.6 mag for both metallicities.

Using the bolometric magnitudes tabulated by Frogel et al. (1990, see also Ferraro et al. (1995, 2004)), LMC and SMC distance moduli of 18.5 and 18.9, respectively, and cluster ages from a variety of compilations (e.g. Da Costa 2002), we have constructed an empirical relationship between AGB tip luminosity and age, for ages older than approximately 1 Gyr. This relation is primarily based on those clusters with extensive near-IR observations, e.g. NGC 1783 (Mould et al. 1989), and naturally, given the lack of such clusters in the LMC, it is dependant solely on SMC clusters for ages beyond 3 Gyr. For ages less than this, however, there is no obvious difference between the two sets of clusters. Further, the relation gives results consistent with the (AGB tip luminosity, age of last significant episode of star formation) results quoted above for the MW dE companions. Our adopted relation is shown as the solid line in Fig. 19, where each vertical sequence of points at fixed age represents all the upper AGB stars for a given

cluster. The MW dE companion data from Table 7 are plotted with open star symbols. For comparison, with dotted line we plot the relation between the AGB tip luminosity and age from Stephens & Frogel (2002), determined by using the stellar evolution models of Bertelli et al. (1994) and the mass-loss prescription of Vassiliadis & Wood (1993).

Using our empirically derived relation, and the assumed AGB tip luminosities (−4.5 for AM 1339-445, and −4.8 for AM 1343-452) we derive epochs of the last significant episode of star formation in these Cen A group dEs as 6.5 ± 1 and 4 ± 1 Gyr, respectively (dashed lines in Fig. 19). The uncertainty in age is determined by ±0.1 mag uncertainty in AGB tip bolometric magnitude, but we note that it does not include uncertainty in the relation between the AGB tip luminosity and age. Clearly use of the Stephens & Frogel (2002) relation would result in somewhat younger ages for the last episode of significant star formation. Nevertheless, we conclude that AM 1339-445 is comparable to the MW satellite Leo II, while AM 1343-452 is comparable to Carina.

While the ubiquitous occurrence of RR Lyrae variables shows that the outlying dE satellites of the MW contain at least some old (age ≥ 10 Gyr) stars (e.g. Held et al. 2001), the stellar populations of these systems, particularly Fornax and Leo I, are dominated by stars of intermediate-age. It is therefore of interest to attempt to estimate the relative importance of the intermediate-age populations in the Cen A group dEs. Clearly the lack of observations reaching substantially fainter than the tip of the red giant branch means that we cannot provide detailed estimates of the star formation histories (cf. Gallart et al. 1999). Nevertheless, we can use simple models to provide some information on the relative importance of the intermediate-age stars. Specifically, we assume that the dwarfs are made up of two discrete populations: one which is old, assumed to be 13 Gyr in age, and one which is of intermediate age with the same metallicity. The intermediate-age population fraction is then estimated from the numbers of candidate upper-AGB stars (11 for AM 1339-445, 12 for AM 1343-452), which are presumed to come only from the intermediate-age population, as a proportion of the number of red giants between the tip of the RGB and 0.3 mag fainter (in I). These stars come from both populations. We denote this ratio by P_{IA}. Using the CMDs of Fig. 13 we find $P_{IA} \approx 0.05$-0.10 for both AM 1339-445 and AM 1343-452.

We use models kindly provided by Claudia Maraston to interpret these ratios. The models (cf. Maraston (1998, 2005); see also Ferraro et al. (2004)) estimate the energetics of any post-main-sequence phase by using the so-called fuel consumption theorem (Renzini & Buzzoni 1986), and have been calibrated with the integrated colours of Magellanic Cloud clusters. Using the models for $[Z/H] = -1.35$, which is appropriate for the dEs given the mean metallicities derived in Sect. 3.3, we calculate values of P_{IA} for ages of the intermediate-age component of 1, 2, 4, 6 and 9 Gyr, and for intermediate-age population fractions varying from 0.0 (i.e. old stars only) to 1.0 (i.e. intermediate-age stars only). In all cases we include in the calculation of the relative number of red giants between I(TRGB) and I(TRGB+0.3) not only first ascent red giants, but also early-AGB stars in the same I magnitude range.

The models indicate that if we assume an age of ∼6.5 Gyr for the intermediate-age population in AM 1339-445, and ∼4 Gyr for AM 1343-452, then the observed values of P_{IA} for the dEs imply intermediate-age population fractions of ∼15% for both galaxies. It is not easy to give an uncertainty for this value, but it most likely a lower limit on the true fraction. For example, the number of upper-AGB candidates is likely to be a lower limit on the actual number, given the selection process and the photometric errors. Similarly, since the models show that relative number of upper-AGB stars per RGB star (first ascent and early-AGB) decreases with increasing age, including an additional intermediate-age population older than that used would result in a larger overall intermediate-age population fraction. It is unlikely, however, that the true intermediate-age population fractions for these dEs are more than a factor of two higher than the limit given.

At ∼15%, or even at ∼30%, these intermediate-age population fractions are notably lower than for the outlying MW dE satellites Fornax and Leo I, where the intermediate-age population fractions are dominant. Even for Leo II, the results of Mighell & Rich (1996) suggest an intermediate-age population fraction of ∼40-50%. The Cen A group dEs appear instead to be more similar to the outlying lower luminosity dE companions of M31.

As regards the comparison of these Cen A group dEs with dEs in the Local Group, two further points can be made. First, we have already noted that the $(B-R)_0$ colours of these two galaxies are typical of those for dEs (Jerjen et al. 2000a). Second, using the photometry of Jerjen et al. (2000a) and our moduli, we estimate that the integrated absolute V magnitudes are −12.6 and −11.5, for AM 1339-445 and AM 1343-452, respectively. With these magnitudes and the average metallicities of −1.4 and −1.6 derived above, both galaxies follow closely the luminosity-metallicity relation defined by the Local Group dEs (Caldwell et al. 1998).

5. Summary and Conclusions

We have presented an analysis of the red giant populations of two dE galaxies in the Cen A group, AM 1339-445 and AM 1343-452, using a combination of near-IR and optical data. Both dEs are distant companions of Cen A, the dominant galaxy of the group.

Using the luminosity of the tip of the RGB we have measured distance moduli of both galaxies, $(m-M)_0(AM1339-445) = 27.74 \pm 0.20$, and $(m-M)_0(AM1343-452) = 27.86 \pm 0.20$, which are in good agreement with previously published values (Karachentsev et al. 2002; Jerjen et al. 2000b). The mean colour of the upper RGB stars is used to determine the mean metallicities of $\langle[Fe/H]\rangle = -1.4 \pm 0.2$ for AM 1339-445 and $\langle[Fe/H]\rangle = -1.6 \pm 0.2$ for AM 1343-452. The integrated colours of these two dEs are similar to those of other dEs and they follow the same luminosity-metallicity relation of the LG dEs.

We find evidence for the presence of intermediate-age upper-AGB stars in both galaxies, with the most luminous of these stars being 0.2-0.3 mag brighter in AM 1343-452, than in

AM 1339-445. The luminosities of these stars indicate that significant star formation continued in AM 1343-452 until an age of ∼4 Gyr as against ∼6.5 Gyr in AM 1339-445. In this respect these Cen A group dEs are similar to the outlying dE satellites of the Milky Way. However, we estimate that the fraction of the total population that is of intermediate-age is perhaps ∼15%, which is significantly less than the dominant intermediate-age populations found in outlying Milky Way dE satellites such as Fornax and Leo I.

With only two galaxies it is premature to draw any definite conclusions regarding our long term goal of investigating the role of environment on the evolution of dE galaxies in the Cen A group (cf. Sect. 1). Nevertheless, it is interesting that despite the rather large distance of both dEs from Cen A, their intermediate-age populations are small and relatively old, particularly when compared to the outer dE satellites of the Milky Way. We must, however, await similar analyses for additional dEs in this group before drawing any inferences from this result.

Acknowledgements. We are grateful to our referee, Ivo Saviane, for many useful suggestions which improved the presentation. We thank service mode support at Paranal for conducting the observations and Dr. Claudia Maraston for providing details from her models. GDaC also thanks Prof. Roger Davies, head of Astrophysics at Oxford University, for hosting a sabbatical visit during which this paper was completed. The research has been supported in part by funds from the Australian Research Council through Discovery Project grant DP0343156. BB thanks the Swiss National Science Foundation for financial support. This publication makes use of data products from the Two Micron All Sky Survey, which is a joint project of the University of Massachusetts and the Infrared Processing and Analysis Center/California Institute of Technology, funded by the National Aeronautics and Space Administration and the National Science Foundation. This research has made use of NASA's Astrophysics Data System Bibliographic Services.

References

Aaronson, M., Gordon, G., Mould, J., Olszewski, E., & Suntzeff, N. 1985, ApJ, 296, L7
Aaronson, M. & Mould, J. 1980, ApJ, 240, 804
Aaronson, M. & Mould, J. 1985, ApJ, 290, 191
Armandroff, T. E., Da Costa, G. S., Caldwell, N., & Seitzer, P. 1993, AJ, 106, 986
Barmby, P., Huchra, J. P., Brodie, J. P., et al. 2000, AJ, 119, 727
Barnes, D. G., Staveley-Smith, L., de Blok, W. J. G., et al. 2001, MNRAS, 322, 486
Battinelli, P. & Demers, S. 2004a, A&A, 418, 33
Battinelli, P. & Demers, S. 2004b, A&A, 417, 479
Bergeat, J., Knapik, A., & Rutily, B. 2002, A&A, 390, 967
Bertelli, G., Bressan, A., Chiosi, C., Fagotto, F., & Nasi, E. 1994, A&AS, 106, 275
Bessell, M. S. & Wood, P. R. 1984, PASP, 96, 247
Brown, T. M., Ferguson, H. C., Smith, E., et al. 2003, ApJ, 592, L17
Caldwell, N., Armandroff, T. E., Da Costa, G. S., & Seitzer, P. 1998, AJ, 115, 535
Cardelli, J. A., Clayton, G. C., & Mathis, J. 1989, ApJ, 345, 245
Cioni, M.-R. L. & Habing, H. J. 2003, A&A, 402, 133
Costa, E. & Frogel, J. A. 1996, AJ, 112, 2607
Cutri, R. M., Skrutskie, M. F., van Dyk, S., et al. 2003, VizieR Online Data Catalog, 2246
Da Costa, G. S. 1997, in ASP Conf. Series, Vol. 116, The Nature of Elliptical Galaxies, ed. M. Arnaboldi, G. S. Da Costa, & P. Saha, 270
Da Costa, G. S. 1998, in Stellar astrophysics for the local group: VIII Canary Islands Winter School of Astrophysics, ed. A. Aparicio, A. Herrero, & F. Sanchez, 351
Da Costa, G. S. 2002, in Extragalactic Star Clusters, IAU Symposium 207, 83
Da Costa, G. S. 2004, Publications of the Astronomical Society of Australia, 21, 366
Da Costa, G. S. 2005, in Near Field Cosmology with dwarf Elliptical galaxies, ed. H. Jerjen & B. Binggeli, IAU Colloquium 198, Cambridge Univ. Press, Cambridge, p. 35
Da Costa, G. S. & Armandroff, T. E. 1990, AJ, 100, 162
Da Costa, G. S., Armandroff, T. E., Caldwell, N., & Seitzer, P. 2000, AJ, 119, 705
Dean, J. F., Warren, P. R., & Cousins, A. W. J. 1978, MNRAS, 183, 569
Demers, S., Battinelli, P., & Letarte, B. 2003, AJ, 125, 3037
Demers, S., Dallaire, M., & Battinelli, P. 2002, AJ, 123, 3428
Dolphin, A. E. 2000a, PASP, 112, 1383
Dolphin, A. E. 2000b, PASP, 112, 1397
Evans, R., Davies, J. I., & Phillipps, S. 1990, MNRAS, 245, 164
Ferraro, F., Montegriffo, P., Origlia, L., & Fusi Pecci, F. 2000, AJ, 119, 1282
Ferraro, F. R., Fusi Pecci, F., Testa, V., et al. 1995, MNRAS, 272, 391
Ferraro, F. R., Origlia, L., Testa, V., & Maraston, C. 2004, ApJ, 608, 772
Frogel, J. A., Mould, J., & Blanco, V. M. 1990, ApJ, 352, 96
Frogel, J. A. & Whitelock, P. A. 1998, AJ, 116, 754
Gallart, C., Freedman, W. L., Aparicio, A., Bertelli, G., & Chiosi, C. 1999, AJ, 118, 2245
Girardi, L., Bertelli, G., Bressan, A., et al. 2002, A&A, 391, 195
Grebel, E. K. 2000, in ESA SP, Vol. 445, Star formation from the small to the large scale, ed. F. Favata, A. Kaas, & A. Wilson, 87
Grebel, E. K., Gallagher, J. S., & Harbeck, D. 2003, AJ, 125, 1926
Guarnieri, D., M., Ortolani, et al. 1998, A&A, 331, 70
Harbeck, D., Gallagher, J. S., & Grebel, E. K. 2004, AJ, 127, 2711
Held, E. V., Clementini, G., Rizzi, L., et al. 2001, ApJ, 562, L39
Hurley-Keller, D., Mateo, M., & Nemec, J. 1998, AJ, 115, 1840
Jerjen, H., Binggeli, B., & Freeman, K. C. 2000a, AJ, 119, 593
Jerjen, H., Freeman, K. C., & Binggeli, B. 2000b, AJ, 119, 166
Kang, A., Sohn, Y.-J., Rhee, J., et al. 2005, A&A, 437, 61
Karachentsev, I. D., Sharina, M. E., Dolphin, A. E., et al. 2002, A&A, 385, 21
Kerschbaum, F., Nowotny, W., Olofsson, H., & Schwarz, H. E. 2004, A&A, 427, 613

Lee, Y.-W., Demarque, P., & Zinn, R. 1990, ApJ, 350, 155
Maraston, C. 1998, MNRAS, 300, 872
Maraston, C. 2005, MNRAS, 362, 799
Marigo, P. 2002, A&A, 387, 507
Marigo, P., Girardi, L., & Chiosi, C. 2003, A&A, 403, 225
Mateo, M. L. 1998, ARA&A, 36, 435
Mayer, L., Governato, F., Colpi, M., et al. 2001, ApJ, 559, 754
Menzies, J., Feast, M., Tanabé, T., Whitelock, P., & Nakada, Y. 2002, MNRAS, 335, 923
Mighell, K. J. & Rich, R. M. 1996, AJ, 111, 777
Mould, J., Kristian, J., Nemec, J., Jensen, J., & Aaronson, M. 1989, ApJ, 339, 84
Mould, J. R., Cannon, R. D., Aaronson, M., & Frogel, J. A. 1982, ApJ, 254, 500
Nowotny, W., Kerschbaum, F., Olofsson, H., & Schwarz, H. E. 2003, A&A, 403, 93
Raimondo, G., Cioni, M.-R. L., Rejkuba, M., & Silva, D. R. 2005, A&A, 438, 521
Rejkuba, M. 2004, A&A, 413, 903
Rejkuba, M., Jerjen, H., Da Costa, G. S., Binggeli, B., & Zoccali, M. 2005, in Near Field Cosmology with dwarf Elliptical galaxies, ed. H. Jerjen & B. Binggeli, IAU Colloquium 198, Cambridge Univ. Press, Cambridge, p. 49
Rejkuba, M., Minniti, D., Bedding, T., & Silva, D. 2001, A&A, 379, 781
Rejkuba, M., Minniti, D., Silva, D., & Bedding, T. 2003, A&A, 411, 351
Renzini, A. & Buzzoni, A. 1986, in ASSL Vol. 122: Spectral Evolution of Galaxies, 195–231
Robin, A. C., Reylé, C., Derrière, S., & Picaud, S. 2003, A&A, 409, 523
Salaris, M. & Girardi, L. 2005, MNRAS, 357, 669
Sarajedini, A., Grebel, E. K., Dolphin, A. E., et al. 2002, ApJ, 567, 915
Saviane, I., Held, E. V., & Bertelli, G. 2000, A&A, 355, 56
Schlegel, D. J., Finkbeiner, D. P., & Davis, M. 1998, ApJ, 500, 525
Sharina, M. E., Puzia, T. H., & Makarov, D. I. 2005, A&A, 442, 85
Stephens, A. W. & Frogel, J. A. 2002, AJ, 124, 2023
Stetson, P. B. 1987, PASP, 99, 191
Stetson, P. B. 1994, PASP, 106, 250
Valenti, E., Ferraro, F. R., & Origilia, L. 2004, MNRAS, 354, 815
van den Bergh, S. 1994, AJ, 107, 1328
van den Bergh, S. 1999, A&AR, 9, 273
van den Bergh, S. 2000, PASP, 112, 529
Vassiliadis, E. & Wood, P. R. 1993, ApJ, 413, 641
Whitelock, P., Marang, F., & Feast, M. 2000, MNRAS, 319, 728
Zinn, R. & West, M. J. 1984, ApJS, 55, 45